Conservative high order semi-Lagrangian finite difference WENO methods for advection in incompressible flow

Jing-Mei Qiu[1] and Chi-Wang Shu [2]

Abstract

In this paper, we propose a semi-Lagrangian finite difference formulation for approximating conservative form of advection equations with general variable coefficients. Compared with the traditional semi-Lagrangian finite difference schemes [4, 21], which approximate the advective form of the equation via direct characteristics tracing, the scheme proposed in this paper approximates the conservative form of the equation. This essential difference makes the proposed scheme naturally conservative for equations with general variable coefficients. The proposed conservative semi-Lagrangian finite difference framework is coupled with high order essentially non-oscillatory (ENO) or weighted ENO (WENO) reconstructions to achieve high order accuracy in smooth parts of the solution and to capture sharp interfaces without introducing spurious oscillations. The scheme is extended to high dimensional problems by Strang splitting. The performance of the proposed schemes is demonstrated by linear advection, rigid body rotation and swirling deformation. As the information is propagating along characteristics, the proposed scheme does not have CFL time step restriction of the Eulerian method, allowing for a more efficient numerical realization for many application problems.

Keywords: advection in incompressible flow; conservative scheme; semi-Lagrangian methods; WENO reconstruction.

[1]Department of Mathematical and Computer Science, Colorado School of Mines, Golden, 80401. E-mail: jingqiu@mines.edu. Research supported by NSF grant number 0914852 and Air Force Office of Scientific Research grant number FA9550-09-1-0344.

[2]Division of Applied Mathematics, Brown University, Providence, 02912. E-mail: shu@dam.brown.edu. Research supported by AFOSR grant FA9550-09-1-0126 and NSF grant DMS-0809086.

1 Introduction

In this paper, we consider numerically simulating the advection of a scalar density function $u(\mathbf{x}, t)$ in an incompressible flow with the specified velocity field $\mathbf{a}(\mathbf{x}, t)$ in general high spatial dimensions, $\mathbf{x} \in \mathcal{R}^d$, where d is the spatial dimension. The evolution of $u(\mathbf{x}, t)$ is governed by the advection equation

$$u_t + \mathbf{a}(\mathbf{x}, t) \cdot \nabla_{\mathbf{x}} u = 0, \tag{1.1}$$

with the divergence free condition on the velocity field $\nabla \cdot \mathbf{a} = 0$. Equation (1.1) can be rewritten in a conservative form as

$$u_t + \nabla_{\mathbf{x}} \cdot (\mathbf{a}(\mathbf{x}, t)u) = 0, \tag{1.2}$$

due to the divergence free condition of the velocity field $\mathbf{a}$.

Numerical approaches in simulating the advection problem described above can be classified as three types: Eulerian, Lagrangian and semi-Lagrangian. The Lagrangian type particle methods evolve the solution by following the trajectories of some sampled macro-particles, while the Eulerian approach evolves the PDE itself, e.g. equation (1.1) or (1.2), on a fixed numerical grid. The semi-Lagrangian approach is a mixed approach of Lagrangian and Eulerian in the sense that it has a fixed numerical grid; however in each time step evolution it evolves the PDEs by propagating information along characteristics. As the Eulerian approach, the semi-Lagrangian method can be designed to be of very high order accuracy [21], an advantage when compared with the Lagrangian approach which suffers the low order $\mathcal{O}(1/\sqrt{N})$, with N being the number of sampling macro-particles, due to the statistical noise in the initial sampling of macro-particles. On the other hand, because of the evolution mechanism, the semi-Lagrangian method does not suffer the CFL time step restriction as in the Eulerian approach, allowing for extra large time step evolution therefore less computational effort. In this paper, a scheme is considered to be semi-Lagrangian, if it has the following three components.

1. A solution space: the solution space can be point values, integrated mass (cell averages), or a piecewise polynomial function living on a fixed numerical grid, corresponding to the semi-Lagrangian finite difference scheme [5, 21, 16], semi-Lagrangian finite volume scheme [13] and the characteristic Galerkin method [7, 18] respectively.

2. In each of the time step evolution, information is propagated along characteristics. In this step, there is no explicit numerical discretization of $\frac{d}{dt}$. The *only* numerical error in time comes from tracing characteristics backward in time in order to find their origin at t^n. Usually, a high order interpolation or reconstruction procedure, which determines the spatial accuracy of the scheme, is applied to recover the information among discrete information on the solution space.

3. Lastly, the evolved solution is projected back onto the solution space, updating the numerical solution at t^{n+1}.

The semi-Lagrangian approach is very popular in the numerical weather prediction [26], the plasma simulations [25, 1, 2, 16, 28, 3, 21], among many others. In the kinetic simulation of plasma, a very popular approach is the Strang split semi-Lagrangian method first proposed by Cheng and Knorr [6]. The idea is that, rather than solving the truly multi-dimensional genuinely nonlinear equations, Cheng and Knorr applied the Strang splitting to decouple the high dimensional nonlinear Vlasov equation into a sequence of 1-D 'linear' equations on a rectangular grid. The advantage of performing such a splitting is that the decoupled 1-D advection equations are linear and are much easier to resolve numerically. On the other hand, the numerical error in time is dominated by the splitting error which is of order $\mathcal{O}(\Delta t^2)$. In this paper, we will adopt the Strang splitting idea, and decouple the high dimensional advection problem (1.2) into a sequence of conservative 1-D advection equation. We remark that in the context of Strang splitting equation (1.1) or (1.2), or the kinetic equation, semi-Lagrangian finite difference schemes that evolve point values would be advantageous when compared with the semi-Lagrangian finite volume schemes or characteristic Galerkin methods. A scheme working on grid points would not suffer the 'at best' second order spatial error, because of the shearing of velocity field, as those schemes working over a cell region. In this paper, we consider the semi-Lagrangian finite difference method with Strang splitting on equation (1.2).

The traditional semi-Lagrangian finite difference schemes [3, 21, 16] usually approximate the advective form of equation by tracing characteristics backward in time and using an interpolation algorithm to recover the information among grid points. For example, in the context of Strang splitting, the equation (1.1) is split into a sequence of 1-D advective

equations

$$u_t + a_i(\mathbf{x}, t)u_{x_i} = 0, \quad i = 1, \cdots, d \tag{1.3}$$

each of which is approximated by a semi-Lagrangian finite difference scheme. Such scheme has decent performance in many problems [3]. However, the total mass, which is an analytically conserved quantity, is not necessarily conserved numerically for such a scheme. This might lead to serious problems, for example in the relativistic Vlasov-Maxwell simulation [16]. In this paper, we consider a new formulation of semi-Lagrangian scheme that approximates the conservative form, rather than the advective form of the PDE. Specifically, in the context of Strang splitting, the equation (1.1) (or equivalently the equation (1.2)) is split into a sequence of 1-D conservative equations

$$u_t + (a_i(\mathbf{x}, t)u)_{x_i} = 0, \quad i = 1, \cdots, d \tag{1.4}$$

each of which is approximated by a conservative scheme.

An important component of the semi-Lagrangian scheme is the interpolation or reconstruction procedure in recovering information among grid points, which determines the spatial accuracy of the scheme. In the literature, there are a variety of choices [12, 28] such as piecewise parabolic method (PPM) [10], positive and flux conservative method (PFC) [13], spline interpolation [11], cubic interpolation propagation (CIP) [27], ENO/WENO interpolation or reconstruction [17, 23, 5, 21]. In this paper, we will apply the ENO or WENO procedures to ensure high order spatial accuracy in smooth regions and to avoid spurious oscillations at discontinuities.

In summary, we propose a new semi-Lagrangian finite difference scheme approximating the conservative form of the 1-D advection equation (1.4) and the multi-D advection equation (1.2) by a conservative Strang splitting. Since most of our discussion will be focused on a split 1-D problem, without loss of generality, we will work on the following 1-D equation

$$u_t + (a(x, t)u)_x = 0. \tag{1.5}$$

We remark that solving the truly multi-dimensional problem, rather than the Strang split 1-D equation, is highly nontrivial and is going to be our future research. On the other hand, there is a recent numerical approach in overcoming the dimensional splitting error in the

framework of spectral deferred correction methods [8]. The idea over there might have the potential of being applied to our split scheme here.

The paper is organized as follows. Section 2 is a review of finite difference WENO scheme coupled with the method of lines procedure. Section 3 gives the semi-Lagrangian scheme for approximating equation (1.5) with $a(x,t)$ being a constant. Section 4 generalizes the scheme to the equations with general variable coefficient $a(x,t)$. Section 5 demonstrates the performance of the proposed schemes by linear advection, rigid body rotation and swirling deformation. Section 6 gives the conclusion and indicates a few possible directions for future research.

2 Review of finite difference WENO scheme coupled with the method of line approach

In this section, we briefly review the finite difference WENO spatial discretization coupled with the method of lines (MOL) procedure for a 1-D conservative form of advection equation (1.5), with the initial condition $u(x,t=0)=u_0(x)$. For simplicity, we assume periodic boundary condition. The purpose of this review section is to recall the idea behind the high order finite difference WENO scheme, especially the sliding average function $h(x)$, which is also used in the proposed semi-Lagrangian finite difference scheme in Sections 3 and 4. The readers are referred to [9, 23] for more details. In this paper, we adopt the following spatial discretization of the domain $[a,b]$

$$a = x_{\frac{1}{2}} < x_{\frac{3}{2}}, \cdots, < x_{N+\frac{1}{2}} = b, \tag{2.1}$$

where $I_i = [x_{i-\frac{1}{2}}, x_{i+\frac{1}{2}}]$, $i = 1, \cdots, N$ are uniform numerical cells with the center of the cell $x_i = \frac{1}{2}(x_{i+\frac{1}{2}} + x_{i-\frac{1}{2}})$ and the cell size $\Delta x = x_{i+\frac{1}{2}} - x_{i-\frac{1}{2}} = (b-a)/N$. We denote $u_i(t) = u(x_i,t)$ and $u_i^n = u(x_i,t^n)$ with $t^n = n\Delta t$.

The finite difference scheme evolves the point values of the solution $\{u_i\}_{i=1}^N$ by approximating the equation (1.5) directly. The scheme is of conservative form

$$\frac{d}{dt}u_i = -\frac{1}{\Delta x}(\hat{f}_{i+\frac{1}{2}} - \hat{f}_{i-\frac{1}{2}}), \tag{2.2}$$

where the numerical flux

$$\hat{f}_{i+\frac{1}{2}} = \hat{f}(u_{i-p}, \cdots, u_{i+q})$$

is consistent with the physical flux $f(u) = a(x,t)u$ and is Lipschitz continuous with respect to all arguments. The stencil $\{u_{i-p}, \cdots, u_{i+q}\}$ is chosen to be upwind biased. Especially, when $a(x,t) \geq 0$, one more point from the left ($p = q$) will be taken to reconstruct $\hat{f}_{i+\frac{1}{2}}$; when $a(x,t) < 0$, one more point from the right ($p = q-2$) will be taken. When $a(x,t)$ changes sign over the domain, then a flux splitting, e.g. the Lax-Friedrich flux splitting can be applied [23]. The spatial accuracy of the scheme is determined by how well $\frac{1}{\Delta x}(\hat{f}_{i+\frac{1}{2}} - \hat{f}_{i-\frac{1}{2}})$ approximates $(a(x,t)u)_x$. To obtain a high order approximation, Shu and Osher [24] introduced a sliding average function $h(x)$, such that

$$\frac{1}{\Delta x}\int_{x-\frac{\Delta x}{2}}^{x+\frac{\Delta x}{2}} h(\xi)d\xi = a(x,t)u(x,t), \tag{2.3}$$

for a fixed t. Taking the x derivative of the above equation gives

$$\frac{1}{\Delta x}\left(h(x+\frac{\Delta x}{2}) - h(x-\frac{\Delta x}{2})\right) = (au)_x. \tag{2.4}$$

Therefore the numerical flux $\hat{f}_{i+\frac{1}{2}}$ in equation (2.2) can be taken as $h(x_{i+\frac{1}{2}})$, which can be reconstructed from neighboring cell averages of $h(x)$, $\bar{h}_j = \frac{1}{\Delta x}\int_{I_j} h(\xi)d\xi \overset{(2.3)}{=} a(x_j,t)u(x_j,t)$, $j = i-p, \cdots, i+q$ by WENO reconstruction [23]. Equation (2.2) is further discretized in time by a method of line (MOL) procedure, the most popular of which is the third order TVD Runge-Kutta method [14].

Remark 2.1. An essential difference between the semi-Lagrangian scheme proposed in this paper and the finite difference WENO reviewed above is the way of evolving solution in time. There is explicit time discretization, e.g. the Runge-Kutta method, in the method of line approach, while in the semi-Lagrangian scheme, there is no explicit discretization of time derivative $\frac{d}{dt}$. Rather, information is propagated along characteristics and the only error in time comes from tracing characteristics backward in time. As a result, the accuracy and stability issues involved in the temporal evolution of semi-Lagrangian scheme are quite different from those in the method of line approach. In this paper, we only consider the situation when the backward characteristic tracing can be performed either exactly (when a is a constant) or by a high order ODE solver (when $a = a(x,t)$).

3 Semi-Lagrangian scheme for 1-D advection with constant coefficient

We start by introducing the proposed semi-Lagrangian formulation for 1-D equation

$$u_t + (au)_x = 0, \tag{3.1}$$

where a is a constant. The formulation presented in this section will be extended to the case of variable coefficient $a = a(x,t)$ in the next section.

3.1 Basic formulation

We propose a semi-Lagrangian finite difference scheme by integrating equation (3.1), which is of conservative form, over $[t^n, t^{n+1}]$,

$$u(x,t^{n+1}) = u(x,t^n) - \left(\int_{t^n}^{t^{n+1}} au(x,\tau)d\tau \right)_x.$$

Evaluating the above equation at the grid point x_i gives

$$\begin{aligned} u_i^{n+1} &= u_i^n - \left(\int_{t^n}^{t^{n+1}} au(x_i,\tau)d\tau \right)_x \\ &= u_i^n - \mathcal{F}_x|_{x=x_i} \end{aligned} \tag{3.2}$$

where we let

$$\mathcal{F}(x) = \int_{t^n}^{t^{n+1}} au(x,\tau)d\tau. \tag{3.3}$$

We introduce a function $\mathcal{H}(x)$, whose sliding average is $\mathcal{F}(x)$, i.e.

$$\mathcal{F}(x) = \frac{1}{\Delta x} \int_{x-\frac{\Delta x}{2}}^{x+\frac{\Delta x}{2}} \mathcal{H}(\xi)d\xi. \tag{3.4}$$

Taking the x derivative of the above equation gives

$$\mathcal{F}_x = \frac{1}{\Delta x} \left(\mathcal{H}(x+\frac{\Delta x}{2}) - \mathcal{H}(x-\frac{\Delta x}{2}) \right).$$

Therefore the equation (3.2) can be written in a conservative form as

$$u_i^{n+1} = u_i^n - \frac{1}{\Delta x}(\mathcal{H}(x_{i+\frac{1}{2}}) - \mathcal{H}(x_{i-\frac{1}{2}})), \tag{3.5}$$

where $\mathcal{H}(x_{i+\frac{1}{2}})$ is called the flux function. Notice that, from equation (3.1) to (3.5) there is no numerical discretization involved yet. Similar to the idea in finite difference WENO scheme, $\mathcal{H}(x_{i+\frac{1}{2}})$ can be reconstructed from its neighboring cell averages

$$\bar{\mathcal{H}}_j = \frac{1}{\Delta x}\int_{x_{j-\frac{1}{2}}}^{x_{j+\frac{1}{2}}} H(\xi)d\xi \overset{(3.4)}{=} \mathcal{F}(x_j), \quad j = i-p, \cdots, i+q. \tag{3.6}$$

Now the remaining question is how to obtain $\{\mathcal{F}(x_i)\}_{i=1}^N$ (or $\{\bar{\mathcal{H}}_i\}_{i=1}^N$).

From Figure 3.1, we observe that, at each of the grid points at time level t^{n+1}, say (x_i, t^{n+1}), there exists a backward characteristic line, with the foot located on time level t^n at $x_i^\star$. When a is constant, these backward characteristic lines are straight and parallel with slope $\frac{1}{a}$ in the x-t plane. Moreover, along each of these characteristic lines the solution remains constant, i.e. $u(x_i, t^{n+1}) = u(x_i^\star, t^n)$, which is the fact used in most of semi-Lagrangian finite difference schemes in the literature. We propose to take a slightly different approach here. We denote the region Ω_i to be the triangular region bounded by the three points (x_i, t^{n+1}), (x_i, t^n) and $(x_i^\star, t^n)$, see Figure 3.1. We apply the integral form of equation (3.1) over the region Ω_i,

$$\int_{\Omega_i} u_t + (au)_x = 0. \tag{3.7}$$

By the Divergence Theorem, the left hand side of the above equation can be written in the following explicit form

$$\begin{aligned}\int_{\Omega_i} u_t + (au)_x &= \int_{\partial\Omega_i} u \cdot n_t + au \cdot n_x \\ &= -\int_{x_i^\star}^{x_i} u(\xi, t^n)d\xi + \int_{t^n}^{t^{n+1}} au(x_i, \tau)d\tau. \end{aligned}\tag{3.8}$$

From equation (3.7) and (3.8),

$$\bar{\mathcal{H}}_i = \mathcal{F}(x_i) = \int_{t^n}^{t^{n+1}} au(x_i, \tau)d\tau = \int_{x_i^\star}^{x_i} u(\xi, t^n)d\xi, \tag{3.9}$$

where $\int_{x_i^\star}^{x_i} u(\xi, t^n)d\xi$ can be reconstructed from $\{u_i^n\}_{i=1}^N$.

In summary, a semi-Lagrangian finite difference scheme in evolving the solution from t^n to t^{n+1} to approximate equation (3.1) can be designed as follows.

Step 1: At each of the grid points at time level t^{n+1}, say (x_i, t^{n+1}), trace the characteristic back to time level t^n at $x_i^\star$. When a is constant, $x_i^\star = x_i - a\Delta t$.

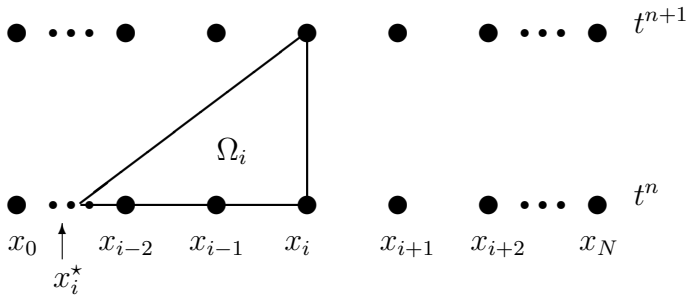

Figure 3.1: Semi-Lagrangian scheme approximates equation (1.5).

Step 2: Reconstruct $\{\bar{\mathcal{H}}_i\}_{i=1}^N$ with $\bar{\mathcal{H}}_i \overset{(3.9)}{=} \int_{x_i^\star}^{x_i} u(\xi, t^n)d\xi$ from $\{u_i^n\}_{i=1}^N$. We use $\mathcal{R}_1$ to denote this reconstruction procedure

$$\bar{\mathcal{H}}_i = \mathcal{R}_1[x_i^\star, x_i](u_{i-p_1}^n, \cdots, u_{i+q_1}^n), \tag{3.10}$$

where $i-p_1, \cdots, i+q_1$ indicate the stencil used in the reconstruction, and $\mathcal{R}_1[a,b]$ indicates the reconstruction of $\int_a^b u(\xi,t)d\xi$.

Step 3: Reconstruct $\{\mathcal{H}(x_{i+\frac{1}{2}})\}_{i=0}^N$ from $\{\bar{\mathcal{H}}_i\}_{i=1}^N$. We use $\mathcal{R}_2$ to denote this reconstruction procedure

$$H(x_{i+\frac{1}{2}}) = \mathcal{R}_2(\bar{\mathcal{H}}_{i-p_2}, \cdots, \bar{\mathcal{H}}_{i+q_2}), \tag{3.11}$$

where $i-p_2, \cdots, i+q_2$ indicate the stencil used in the reconstruction.

Step 4: Update the solution $\{u_i^{n+1}\}_{i=1}^N$ by equation (3.5) with $H(x_{i\pm\frac{1}{2}})$ computed in the previous step.

Remark 3.1. In the proposed scheme, the propagation of the information along characteristics is not as explicit as those in the traditional semi-Lagrangian finite difference scheme $u_i^{n+1} = u(x_i^\star, t^n)$. However, by applying the Divergence Theorem on equation (3.7), the information on $[x_i^\star, x_i] \times t^n$ is propagated over to the region of $\{x_i\} \times [t^n, t^{n+1}]$. Such propagation of information is in the spirit of semi-Lagrangian. When a is constant, there is no error in locating the root of characteristic $x_i^\star$, therefore there is no error in time at all in the proposed scheme. The accuracy of the scheme is solely determined by the spatial reconstruction procedure outlined in Steps 2 and 3 above.

Remark 3.2. The basic formulation of the scheme above can be generalized to the case when a is a variable coefficient $a(x,t)$ without difficulty, see Section 4.

In the following two subsections, we discuss the situation when a first order (Section 3.2) and general high order (Section 3.3) spatial reconstructions are applied to recover the information between grid point values.

3.2 A first order scheme

To better understand the scheme, we start with a first order reconstruction, which is discussed as two separate cases $|a|\Delta t \leq \Delta x$ and $|a|\Delta t > \Delta x$. Despite its simplicity, the first order scheme gives us insight in designing the high order extension in Section 3.3.

The procedure for a first order scheme can be designed as following. In Step 2, we reconstruct $\bar{\mathcal{H}}_i = \int_{x_i^\star}^{x_i} u(\xi, t^n) d\xi$ where the underlying function $u(x,t^n)$ is approximated by a piecewise constant function

$$u(x,t^n) = u_i^n, \quad \text{on} \quad [x_{i-1}, x_i], \tag{3.12}$$

and in Step 3, we design the flux

$$\mathcal{H}(x_{i+\frac{1}{2}}) = \bar{\mathcal{H}}_i, \tag{3.13}$$

regardless of the sign of a.

1. Consider $|a|\Delta t \leq \Delta x$. When $a \geq 0$, $x_i^\star \leq x_i$, then

$$\mathcal{H}(x_{i+\frac{1}{2}}) = \bar{\mathcal{H}}_i = \int_{x_i^\star}^{x_i} u(\xi, t^n) d\xi \approx (x_i - x_i^\star) u_i^n = a\Delta t u_i^n.$$

Plug these flux functions into equation (3.5) gives the scheme

$$u_i^{n+1} = u_i^n - \frac{a\Delta t}{\Delta x}(u_i^n - u_{i-1}^n) = u_i^n - \xi(u_i^n - u_{i-1}^n), \tag{3.14}$$

where $\xi = \frac{a\Delta t}{\Delta x}$. The scheme reduces to the prototype of the first order finite difference upwind scheme. Especially when $a\Delta t = \Delta x$, the scheme in equation (3.14) reduces to $u_i^{n+1} = u_{i-1}^n$, indicating the exact shifting of grid points. In this case, the solution is exactly evolved, with no numerical error in either time or space. Similar result holds when $a < 0$ and $x_i^\star > x_i$. Plug flux functions

$$\mathcal{H}(x_{i+\frac{1}{2}}) = \bar{\mathcal{H}}_i = \int_{x_i}^{x_i^\star} u(\xi, t^n) d\xi \approx (x_i^\star - x_i) u_{i+1}^n = |a|\Delta t u_{i+1}^n$$

into equation (3.5) gives

$$u_i^{n+1} = u_i^n + \xi(u_{i+1}^n - u_i^n), \tag{3.15}$$

with $\xi = \frac{|a|\Delta t}{\Delta x}$, which is the prototype of the first order finite difference upwind scheme. Especially when $|a|\Delta t = \Delta x$, the scheme reduces to $u_i^{n+1} = u_{i+1}^n$.

2. Consider $|a|\Delta t > \Delta x$. When $a \geq 0$ and $x_i - x_i^\star > \Delta x$. Let $i^\star$ to be the index such that $x_i^\star \in (x_{i^\star-1}, x_{i^\star}]$ and $\xi = \frac{x_{i^\star} - x_i^\star}{\Delta x}$

$$\mathcal{H}(x_{i+\frac{1}{2}}) = \bar{\mathcal{H}}_i = \int_{x_i^\star}^{x_i} u(\xi, t^n) d\xi \approx \sum_{j=i^\star+1}^{i} u_j^n \Delta x + (x_{i^\star} - x_i^\star) u_{i^\star}^n$$

Plug these flux functions into equation (3.5) gives the scheme

$$\begin{aligned} u_i^{n+1} &= u_i^n - \frac{1}{\Delta x}\left((\sum_{j=i^\star+1}^{i} u_j^n \Delta x + (x_{i^\star} - x_i^\star) u_{i^\star}^n) - (\sum_{j=i^\star}^{i-1} u_j^n \Delta x + (x_{i^\star-1} - x_{i-1}^\star) u_{i^\star-1}^n) \right) \\ &= u_i^n - \frac{1}{\Delta x}(\Delta x(u_i^n - u_{i^\star}^n) + \xi \Delta x(u_{i^\star}^n - u_{i^\star-1}^n)) \\ &= u_{i^\star}^n - \xi(u_{i^\star}^n - u_{i^\star-1}^n) \end{aligned} \tag{3.16}$$

One observation from the equation above is that, although information is integrated along $x_i^\star$ to x_i to compute $\bar{\mathcal{H}}_i$, the final form of the scheme (3.16) only involves the information around the foot of characteristics $x_i^\star$. Similar result holds for $a < 0$.

Remark 3.3. In our scheme, neither the reconstruction $\mathcal{R}_1$ nor $\mathcal{R}_2$ depends on the wind direction (the sign of $a(x,t)$). The information on wind direction is automatically recovered by locating $x_i^\star$ via characteristics tracing, see the derivation of equation (3.14) and (3.15). This consistent treatment regardless of the sign of a is crucial, when dealing with the situation that $a(x,t)$ changes sign in Section 4.

Remark 3.4. Another symmetric way of approximation can be designed as following. In Step 2, the underlying function $u(x, t^n)$ is approximated by a piecewise constant function $u(x, t^n) = u_{i-1}^n$, on $[x_{i-1}, x_i]$; and in Step 3, $\mathcal{H}(x_{i+\frac{1}{2}}) = \bar{\mathcal{H}}_{i+1}$, regardless of the sign of a. With this approximation, the first order semi-Lagrangian scheme ends up to be the same as that from the reconstruction (3.12) and (3.13), i.e. equation (3.14) for $a \geq 0$ and equation (3.15) for $a < 0$.

3.3 High order schemes with WENO reconstructions

In this section, we will extend the first order scheme in the previous section to high order. We will first consider the case when $|a|\Delta t < \Delta x$, in which we will first consider linear high order extension of the scheme for smooth problem. Then we will incorporate the WENO mechanism to deal with solutions with discontinuities. After that we will extend the scheme to the case when $|a|\Delta t \geq \Delta x$. The algorithm is summarized in Section 3.3.4. In this subsection, we will focus our discussion on the case of $a \geq 0$. For the case of $a < 0$, we will omit the details of the reconstruction procedure for brevity, but only provide necessary formulas for implementation convenience.

3.3.1 High order linear reconstructions: $|a|\Delta t < \Delta x$

To extend the first order scheme to high order, we would like to make the reconstruction operators $\mathcal{R}_1$ and $\mathcal{R}_2$ in equation (3.10) and (3.11) to be of high order. A direct way of doing this is to include more points in the reconstruction stencil in (3.10) and (3.11). Take a third order scheme for example. We will extend the reconstruction (3.12) by using $\{u^n_{i-1}, u^n_i, u^n_{i+1}\}$ as the reconstruction stencil to reconstruct $u(x, t^n)$ on $[x_{i-1}, x_i]$; we will extend (3.13) by using $\{\mathcal{H}_{i-1}, \mathcal{H}_i, \mathcal{H}_{i+1}\}$ as the reconstruction stencil, regardless of the sign of the advection coefficient a. One problem with such implementation is that the reconstruction stencil is too widely spread. Specifically, when $a \geq 0$ and $a\Delta t \leq \Delta x$, five points $\{u_{i-2}, u_{i-1}, u_i, u_{i+1}, u_{i+2}\}$ are involved to reconstruct the third order flux function $\mathcal{H}(x_{i+\frac{1}{2}})$. More seriously, the scheme is linearly unstable. To remedy the problem, we observe that in the case of linear reconstruction, the operators $\mathcal{R}_1$ and $\mathcal{R}_2$ can be combined together as a linear operator $\mathcal{R} = \mathcal{R}_2 \circ \mathcal{R}_1$,

$$\mathcal{H}(x_{i+\frac{1}{2}}) = \mathcal{R}(u^n_{i-p}, \cdots, u^n_{i+q}) \tag{3.17}$$

where $i - p, \cdots, i + q$ indicate the reconstruction stencil. Such compression of two linear operators not only makes the reconstruction stencil more compact, but also provides a stable scheme. Below, we will use third and fifth order reconstructions as examples to illustrate the reconstruction procedure. The formulas are also a good reference for implementation purpose.

Third order linear reconstruction. When $a \geq 0$, we will use the three-point stencil

$\{u_{i-1}, u_i, u_{i+1}\}$ to reconstruct $\bar{\mathcal{H}}_j$ with $j = i-1, i, i+1$ respectively, from which we reconstruct $\mathcal{H}(x_{i+\frac{1}{2}})$ with third order. Specifically, we integrate the quadratic polynomial interpolating x_{i-1}, x_i, x_{i+1} over $[x_j^\star, x_j] = [x_j - \xi\Delta x, x_j]$ as approximation to $\bar{\mathcal{H}}_j$, with $j = i-1, i, i+1$, where $\xi = \frac{a\Delta t}{\Delta x}$.

$$\begin{aligned}
\bar{\mathcal{H}}_{i-1} = \Delta x \Bigg(& (-\frac{5}{12} - \frac{1}{6}(-\xi - 1)^3 + \frac{1}{4}(-\xi - 1)^2) u_{i-1}^n \\
& + (\xi + \frac{1}{3} + \frac{1}{3}(-\xi - 1)^3) u_i^n \\
& + (\frac{1}{12} - \frac{1}{6}(-\xi - 1)^3 - \frac{1}{4}(-\xi - 1)^2) u_{i+1}^n \Bigg) \qquad (3.18) \\
\bar{\mathcal{H}}_i = \Delta x \Bigg(& (\frac{1}{6}\xi^3 + \frac{1}{4}\xi^2) u_{i-1}^n + (\xi - \frac{1}{3}\xi^3) u_i^n + (\frac{1}{6}\xi^3 - \frac{1}{4}\xi^2) u_{i+1}^n \Bigg) \qquad (3.19) \\
\bar{\mathcal{H}}_{i+1} = \Delta x \Bigg(& (-\frac{1}{12} - \frac{1}{6}(1 - \xi)^3 + \frac{1}{4}(1 - \xi)^2) u_{i-1}^n \\
& + (\xi - \frac{1}{3} + \frac{1}{3}(1 - \xi)^3) u_i^n \\
& + (\frac{5}{12} - \frac{1}{6}(1 - \xi)^3 - \frac{1}{4}(1 - \xi)^2) u_{i+1}^n \Bigg), \qquad (3.20)
\end{aligned}$$

and, as in the linear reconstruction in the finite difference WENO scheme,

$$\mathcal{H}(x_{i+\frac{1}{2}}) = -\frac{1}{6}\bar{\mathcal{H}}_{i-1} + \frac{5}{6}\bar{\mathcal{H}}_i + \frac{1}{3}\bar{\mathcal{H}}_{i+1}. \qquad (3.21)$$

Plugging equations (3.18)-(3.20) into equation (3.21) gives

$$\begin{aligned}
\mathcal{H}(x_{i+\frac{1}{2}}) &= \mathcal{R}(u_{i-1}^n, u_i^n, u_{i+1}^n) \\
&= \Delta x \left((\frac{1}{6}\xi^3 - \frac{1}{6}\xi) u_{i-1}^n + (-\frac{1}{3}\xi^3 + \frac{1}{2}\xi^2 + \frac{5}{6}\xi) u_i^n + (\frac{1}{6}\xi^3 - \frac{1}{2}\xi^2 + \frac{1}{3}\xi) u_{i+1}^n \right) \\
&\doteq \Delta x (C_1^3 u_{i-1}^n + C_2^3 u_i^n + C_3^3 u_{i+1}^n). \qquad (3.22)
\end{aligned}$$

When $a < 0$, we will use the three-point stencil $\{u_i, u_{i+1}, u_{i+2}\}$ to reconstruct $\bar{\mathcal{H}}_j$ with $j = i-1, i, i+1$ respectively, from which we reconstruct $\mathcal{H}(x_{i+\frac{1}{2}})$ with third order. Specifically, we integrate the quadratic polynomial interpolating x_i, x_{i+1}, x_{i+2} over $[x_j, x_j^\star] = [x_j, x_j + \xi\Delta x]$ as approximation to $\bar{\mathcal{H}}_j$, with $j = i-1, i, i+1$, where $\xi = \frac{|a|\Delta t}{\Delta x}$. Then we reconstruct $\mathcal{H}(x_{i+\frac{1}{2}})$ by a linear reconstruction as in equation (3.21). In the end,

$$\mathcal{H}(x_{i+\frac{1}{2}}) = \mathcal{R}(u_i^n, u_{i+1}^n, u_{i+2}^n) = -\Delta x (C_3^3 u_i^n + C_2^3 u_{i+1}^n + C_1^3 u_{i+2}^n),$$

with C_i^3, $i = 1, 2, 3$ as defined in equation (3.22), due to the symmetry of the reconstruction. Details of the reconstruction are omitted here for brevity.

Remark 3.5. In the third order reconstruction, we always use the three-point stencil $\{\bar{\mathcal{H}}_{i-1}, \bar{\mathcal{H}}_i, \bar{\mathcal{H}}_{i+1}\}$ to reconstruct $\mathcal{H}(x_{i+\frac{1}{2}})$, regardless the sign of advection coefficient a. We use the stencil $\{u_{i-1}, u_i, u_{i+1}\}$ when $a \geq 0$ and use $\{u_i, u_{i+1}, u_{i+2}\}$ when $a < 0$ to reconstruct $\bar{\mathcal{H}}_j$ with $j = i-1, i, i+1$, due to the location of $x_i^\star$. Similar algorithm is designed for the fifth order linear reconstruction below.

Fifth order linear reconstruction. Similar procedures can be applied for a fifth order reconstruction. For brevity, we only present the reconstruction formulas needed in the actual implementation. When $a \geq 0$, we will take the five-point stencil $\{u_{i-2}, \cdots, u_{i+2}\}$ to reconstruct $\mathcal{H}(x_{i+\frac{1}{2}})$,

$$\begin{aligned}
\mathcal{H}(x_{i+\frac{1}{2}}) &= \mathcal{R}(u_{i-2}^n, u_{i-1}^n, u_i^n, u_{i+1}^n, u_{i+2}^n) \\
&= \Delta x \left((\frac{1}{30}\xi - \frac{1}{24}\xi^3 + \frac{1}{120}\xi^5) u_{i-2}^n \right. \\
&+ (-\frac{13}{60}\xi - \frac{1}{24}\xi^2 + \frac{1}{4}\xi^3 + \frac{1}{24}\xi^4 - \frac{1}{30}\xi^5) u_{i-1}^n \\
&+ (\frac{47}{60}\xi + \frac{5}{8}\xi^2 - \frac{1}{3}\xi^3 - \frac{1}{8}\xi^4 + \frac{1}{20}\xi^5) u_i^n \\
&+ (\frac{9}{20}\xi - \frac{5}{8}\xi^2 + \frac{1}{12}\xi^3 + \frac{1}{8}\xi^4 - \frac{1}{30}\xi^5) u_{i+1}^n \\
&\left. + (-\frac{1}{20}\xi + \frac{1}{24}\xi^2 + \frac{1}{24}\xi^3 - \frac{1}{24}\xi^4 + \frac{1}{120}\xi^5) u_{i+2}^n \right) \\
&\doteq \Delta x (C_1^5 u_{i-2}^n + C_2^5 u_{i-1}^n + C_3^5 u_i^n + C_4^5 u_{i+1}^n + C_5^5 u_{i+2}^n). \qquad (3.23)
\end{aligned}$$

where $\xi = \frac{a\Delta t}{\Delta x}$. When $a < 0$, we will take the five-point stencil $\{u_{i-1}, \cdots, u_{i+3}\}$ to reconstruct $\mathcal{H}(x_{i+\frac{1}{2}})$,

$$\mathcal{H}(x_{i+\frac{1}{2}}) = \mathcal{R}(u_{i-1}^n, u_i^n, u_{i+1}^n, u_{i+2}^n, u_{i+3}^n) = -\Delta x (C_5^5 u_{i-1}^n + C_4^5 u_i^n + C_3^5 u_{i+1}^n + C_2^5 u_{i+2}^n + C_1^5 u_{i+3}^n),$$

where $\xi = \frac{|a|\Delta t}{\Delta x}$ and C_i^5, $i = 1, \cdots, 5$ are as defined in equation (3.23), due to the symmetry of the reconstruction.

Remark 3.6. Assume $a \geq 0$, when $a\Delta t = \Delta x$ (or $\xi = 1$), it can be checked that $\mathcal{H}(x_{i+\frac{1}{2}}) = \Delta x u_i^n$ in both the third order reconstruction (3.22) and the fifth order reconstruction (3.23). Thus the scheme in equation (3.5) reduces to $u_i^{n+1} = u_{i-1}^n$, indicating the exact shifting of grid points. In this case, the solution is exactly evolved, with no numerical error in either time or space. Indeed, it is proved in Proposition 3.7 below that for general high order

reconstructions, such exact evolution is true when $a\Delta t = \Delta x$. Similar conclusion applies when $a < 0$.

Proposition 3.7. Assuming $a \geq 0$, when $a\Delta t = \Delta x$, the flux function $\mathcal{H}(x_{i+\frac{1}{2}}) = \Delta x u_i$ for linear reconstructions of any odd order. In other words, the operator $\mathcal{R}$ in equation (3.17) satisfies

$$\mathcal{R}(u^n_{i-p}, \cdots, u^n_{i+q}) = \Delta x u^n_i, \quad \text{if} \quad a\Delta t = \Delta x$$

for any reconstruction of an odd order $2k+1$. Therefore the scheme (3.5) is reduced to $u^{n+1}_i = u^n_{i-1}$, indicating the exact shifting of grid points. Similar conclusion applies when $a < 0$.

Proof. It is known by definition that

$$\bar{\mathcal{H}}_i = \frac{1}{\Delta x} \int_{x_{i-\frac{1}{2}}}^{x_{i+\frac{1}{2}}} \mathcal{H}(\xi, t) d\xi, \quad i = 1, \cdots N. \tag{3.24}$$

Also when $a\Delta t = \Delta x$,

$$\bar{\mathcal{H}}_i = \int_{x_i^\star}^{x_i} u(\xi, t) d\xi = \int_{x_{i-1}}^{x_i} u(\xi, t) d\xi, \quad i = 1, \cdots N. \tag{3.25}$$

Let $j = i - 1 - k$. To reconstruct $\mathcal{H}(x_{i+\frac{1}{2}})$ with order $2k+1$, we construct a polynomial $P_{2k+1}(x)$ of degree $2k+1$ interpolating the primitive function of $\mathcal{H}$ at $2k+2$ neighboring points $\{x_{j+\frac{1}{2}}, \cdots x_{j+2k+1+\frac{1}{2}}\}$,

$$P_{2k+1}(x_{j+l+\frac{1}{2}}) = \int^{x_{j+l+\frac{1}{2}}} \mathcal{H} d\xi, \quad l = 0, \cdots, 2k+1;$$

then we use $P'_{2k+1}(x_{i+\frac{1}{2}})$ to approximate $\mathcal{H}(x_{i+\frac{1}{2}})$. On the other hand, there is a polynomial $Q_{2k+1}(x)$ of degree $2k+1$ interpolating the primitive function of $\Delta x u$ at $2k+2$ neighboring points $\{x_j, \cdots x_{j+2k+1}\}$,

$$Q_{2k+1}(x_{j+l}) = \Delta x \int^{x_{j+l}} u d\xi, \quad l = 0, \cdots, 2k+1.$$

From equation (3.24) and (3.25),

$$P_{2k+1}(x_{j+l+\frac{1}{2}}) = Q_{2k+1}(x_{j+l}), \quad l = 0, \cdots, 2k+1.$$

Since $P_{2k+1}(x)$ and $Q_{2k+1}(x)$ are both polynomials of degree $2k+1$,

$$P_{2k+1}(x + \frac{\Delta x}{2}) \equiv Q_{2k+1}(x).$$

Taking the x derivative of above equation and evaluate it at x_i gives

$$P'_{2k+1}(x_{i+\frac{1}{2}}) = Q'_{2k+1}(x_i) = \Delta x u(x_i).$$

Therefore, the numerical flux function $\mathcal{H}(x_{i+\frac{1}{2}}) = \Delta x u(x_i)$. Plugging the flux function into equation (3.5) gives $u_i^{n+1} = u_{i-1}^n$, indicating the exact shifting of grid points. This completes the proof. □

3.3.2 High order WENO reconstructions

In general, high order fixed stencil reconstruction of numerical fluxes performs well when the solution is smooth. However, around discontinuities, spurious oscillations will be introduced. In the following, a nonlinear WENO procedure is introduced for reconstructing $\mathcal{H}(x_{i+\frac{1}{2}})$. By adaptively assigning weights to neighboring candidate stencils, the WENO nonlinear reconstruction preserves high order accuracy of the linear scheme around smooth regions of the solution, while producing a sharp and essentially non-oscillatory capture of discontinuities. The WENO reconstruction could also be understood as a black box filtering procedure, based on the fluxes generated from fixed stencil reconstruction introduced above. The original third and fifth order WENO reconstructions, in the finite difference and finite volume framework, were introduced in [20, 17]. In the following, we give the procedure for coupling the high order linear reconstructions in Section 3.3.1 with WENO, by working with a third order and a fifth order WENO reconstruction as examples.

Third order WENO reconstruction. The WENO mechanism is to be coupled with the third order linear reconstruction. When $a \geq 0$, from equation (3.22), the point values $\{u_{i-1}^n, u_i^n, u_{i+1}^n\}$ are used to construct the flux function $\mathcal{H}(x_{i+\frac{1}{2}})$. The flux $\mathcal{H}(x_{i+\frac{1}{2}})$ is composed of information from two potential stencils

$$S_1 = \{u_{i-1}^n, u_i^n\} \text{ and } \quad S_2 = \{u_i^n, u_{i+1}^n\}. \tag{3.26}$$

Intuitively, in regions where the function is smooth, we want to use information from both stencils S_1 and S_2, to obtain a third order approximation. On the other hand, around

a big jump, we only want to use one of the stencils. For example, consider the jump $(u^n_{i-1}, u^n_i, u^n_{i+1}) = (0, 0, 1)$, we only want to use the stencil S_1 to construct the flux function $\mathcal{H}(x_{i+\frac{1}{2}})$, since excluding the stencil S_2 will prevent numerical oscillations. We will use the same idea to construct $\mathcal{H}(x_{i+\frac{1}{2}})$.

1. Compute two second order reconstructions from two stencils S_1 and S_2,

$$\mathcal{H}^{(1)}(x_{i+\frac{1}{2}}) = \Delta x \left((-\frac{1}{2}\xi + \frac{1}{2}\xi^2) u^n_{i-1} + (-\frac{1}{2}\xi^2 + \frac{3}{2}\xi) u^n_i \right) \tag{3.27}$$

$$\mathcal{H}^{(2)}(x_{i+\frac{1}{2}}) = \Delta x \left((\frac{1}{2}\xi + \frac{1}{2}\xi^2) u^n_i + (-\frac{1}{2}\xi^2 + \frac{1}{2}\xi) u^n_{i+1} \right), \tag{3.28}$$

   where $\mathcal{H}^{(1)}(x_{i+\frac{1}{2}})$ is reconstructed from the two-point stencil $\{\bar{\mathcal{H}}_{i-1}, \bar{\mathcal{H}}_i\}$, each of which is reconstructed from the stencil S_1, and $\mathcal{H}^{(2)}(x_{i+\frac{1}{2}})$ is reconstructed from the two-point stencil $\{\bar{\mathcal{H}}_i, \bar{\mathcal{H}}_{i+1}\}$, each of which is reconstructed from the stencil S_2.

2. Compute the linear weights, γ_1 and γ_2, such that

$$\mathcal{H}(x_{i+\frac{1}{2}}) = \gamma_1 \mathcal{H}^{(1)}(x_{i+\frac{1}{2}}) + \gamma_2 \mathcal{H}^{(2)}(x_{i+\frac{1}{2}}). \tag{3.29}$$

   From equation (3.22),

$$\gamma_1 = \frac{1}{3}(1 + \xi), \quad \gamma_2 = \frac{1}{3}(2 - \xi). \tag{3.30}$$

   Note that γ_1 and γ_2 are both positive, if $\xi \in [0, 1]$, which is an important condition of non-oscillatory performance of WENO algorithm [22, 23].

3. Compute the smoothness indicator β_r for each stencil S_r, $r = 1, 2$. The smoothness indicators β_r are designed such that, if the function is smooth over the stencil S_r, then $\beta_r = \mathcal{O}(\Delta x^2)$, but if the function has a discontinuity, then $\beta_r = \mathcal{O}(1)$. For the third order fluxes, the smoothness indicators are,

$$\beta_1 = (u^n_{i-1} - u^n_i)^2, \quad \beta_2 = (u^n_i - u^n_{i+1})^2.$$

4. Compute the nonlinear weights w_1 and w_2. Let

$$\tilde{w}_r = \gamma_r / (\epsilon + \beta_r)^2, \quad r = 1, 2,$$

where ϵ is a small number to prevent the denominator from becoming zero. In our numerical tests we take ϵ to be 10^{-6}. The resulting nonlinear weights are renormalized as,

$$w_r = \tilde{w}_r / \sum_i \tilde{w}_i, \quad r = 1, 2.$$

5. Compute numerical fluxes constructed in WENO fashion.

$$\mathcal{H}(x_{i+\frac{1}{2}}) = w_1 \mathcal{H}^{(1)}(x_{i+\frac{1}{2}}) + w_2 \mathcal{H}^{(2)}(x_{i+\frac{1}{2}}).$$

When $a < 0$, similar WENO procedures can be applied. Below, we provide main formulas that are different from the case of $a \geq 0$, as needed for implementation purpose. Let $\xi = \frac{|a|\Delta t}{\Delta x}$,

$$\mathcal{H}^{(1)}(x_{i+\frac{1}{2}}) = -\Delta x \left((-\frac{1}{2}\xi^2 + \frac{1}{2}\xi) u_i^n + (\frac{1}{2}\xi + \frac{1}{2}\xi^2) u_{i+1}^n \right) \tag{3.31}$$

$$\mathcal{H}^{(2)}(x_{i+\frac{1}{2}}) = -\Delta x \left((-\frac{1}{2}\xi^2 + \frac{3}{2}\xi) u_{i+1}^n + (-\frac{1}{2}\xi + \frac{1}{2}\xi^2) u_{i+2}^n \right) \tag{3.32}$$

$$\gamma_1 = \frac{1}{3}(2 - \xi), \quad \gamma_2 = \frac{1}{3}(1 + \xi)$$

$$\beta_1 = (u_i^n - u_{i+1}^n)^2, \quad \beta_2 = (u_{i+1}^n - u_{i+2}^n)^2.$$

Fifth order WENO reconstruction. The WENO mechanism is to be coupled with the fifth order linear reconstruction. From equation (3.23), the point values $\{u_{i-2}^n, u_{i-1}^n, u_i^n, u_{i+1}^n, u_{i+2}^n\}$ are used to construct the flux function $\mathcal{H}(x_{i+\frac{1}{2}})$. The flux $\mathcal{H}(x_{i+\frac{1}{2}})$ is composed of the information from three potential stencils

$$S_1 = \{u_{i-2}^n, u_{i-1}^n, u_i^n\} \qquad S_2 = \{u_{i-1}^n, u_i^n, u_{i+1}^n\} \text{ and } \qquad S_3 = \{u_i^n, u_{i+1}^n, u_{i+2}^n\}.$$

The fifth order WENO reconstruction of $\mathcal{H}(x_{i+\frac{1}{2}})$ follows the procedure outlined below.

1. Compute third order reconstructions from three stencils S_1, S_2 and S_3,

$$\mathcal{H}^{(1)}(x_{i+\frac{1}{2}}) = \Delta x \left((\frac{1}{6}\xi^3 - \frac{1}{2}\xi^2 + \frac{1}{3}\xi) u_{i-2}^n + (-\frac{1}{3}\xi^3 + \frac{3}{2}\xi^2 - \frac{7}{6}\xi) u_{i-1}^n + (\frac{1}{6}\xi^3 - \xi^2 + \frac{11}{6}\xi) u_i^n \right) \tag{3.33}$$

$$\mathcal{H}^{(2)}(x_{i+\frac{1}{2}}) = \Delta x \left((\frac{1}{6}\xi^3 - \frac{1}{6}\xi) u_{i-1}^n + (-\frac{1}{3}\xi^3 + \frac{1}{2}\xi^2 + \frac{5}{6}\xi) u_i^n + (\frac{1}{6}\xi^3 - \frac{1}{2}\xi^2 + \frac{1}{3}\xi) u_{i+1}^n \right) \tag{3.34}$$

$$\mathcal{H}^{(3)}(x_{i+\frac{1}{2}}) = \Delta x \left((\frac{1}{6}\xi^3 + \frac{1}{2}\xi^2 + \frac{1}{3}\xi) u_i^n + (-\frac{1}{3}\xi^3 - \frac{1}{2}\xi^2 + \frac{5}{6}\xi) u_{i+1}^n + (\frac{1}{6}\xi^3 - \frac{1}{6}\xi) u_{i+2}^n \right), \tag{3.35}$$

where $\mathcal{H}^{(j)}(x_{i+\frac{1}{2}})$ is reconstructed from the three-point stencil $\{\bar{\mathcal{H}}_{i+j-3}, \bar{\mathcal{H}}_{i+j-2}, \bar{\mathcal{H}}_{i+j-1}\}$, each of which is reconstructed from the stencil S_j for $j = 1, 2, 3$.

2. Compute the linear weights γ_1, γ_2 and γ_3, such that

$$\mathcal{H}(x_{i+\frac{1}{2}}) = \gamma_1 \mathcal{H}^{(1)}(x_{i+\frac{1}{2}}) + \gamma_2 \mathcal{H}^{(2)}(x_{i+\frac{1}{2}}) + \gamma_3 \mathcal{H}^{(3)}(x_{i+\frac{1}{2}}).$$

From equation (3.23) and (3.33)-(3.35)

$$\begin{aligned}
\gamma_1 &= \frac{1}{10} + \frac{3}{20}\xi + \frac{1}{20}\xi^2, \\
\gamma_2 &= \frac{3}{5} + \frac{1}{10}\xi - \frac{1}{10}\xi^2, \\
\gamma_3 &= \frac{3}{10} - \frac{1}{4}\xi + \frac{1}{20}\xi^2.
\end{aligned}$$

Note that γ_1, γ_2 and γ_3 are all positive, if $\xi \in [0, 1]$, which is an important condition of non-oscillatory performance of WENO algorithm [22, 23].

3. Compute the smoothness indicator β_r for each stencil S_r, $r = 1, 2, 3$ by

$$\beta_r = \sum_{l=1}^{k} \int_{x_{i-\frac{1}{2}}}^{x_{i+\frac{1}{2}}} \Delta x^{2l-1} \left(\frac{\partial^l p_r(x)}{\partial x^l} \right)^2 dx,$$

where $p_r(x)$ is the reconstruction polynomial from the stencil S_r. Especially, in the case of fifth order WENO reconstruction,

$$\begin{aligned}
\beta_1 &= \frac{13}{12}(u_{i-2}^n - 2u_{i-1}^n + u_i^n)^2 + \frac{1}{4}(u_{i-2}^n - 4u_{i-1}^n + 3u_i^n)^2, \\
\beta_2 &= \frac{13}{12}(u_{i-1}^n - 2u_i^n + u_{i+1}^n)^2 + \frac{1}{4}(u_{i-1}^n - u_{i+1}^n)^2, \\
\beta_3 &= \frac{13}{12}(u_i^n - 2u_{i+1}^n + u_{i+2}^n)^2 + \frac{1}{4}(3u_i^n - 4u_{i+1}^n + u_{i+2}^n)^2.
\end{aligned}$$

4. Compute the nonlinear weights w_1 and w_2. Let

$$\tilde{w}_r = \gamma_r / (\epsilon + \beta_r)^2, \quad r = 1, 2, 3,$$

where ϵ is a small number to prevent the denominator from becoming zero. In our numerical tests we take ϵ to be 10^{-6}. The resulting nonlinear weights are renormalized as

$$w_r = \tilde{w}_r / \sum_i \tilde{w}_i, \quad r = 1, 2, 3.$$

5. Compute numerical fluxes constructed in WENO fashion.

$$\mathcal{H}(x_{i+\frac{1}{2}}) = w_1\mathcal{H}^{(1)}(x_{i+\frac{1}{2}}) + w_2\mathcal{H}^{(2)}(x_{i+\frac{1}{2}}) + w_3\mathcal{H}^{(3)}(x_{i+\frac{1}{2}}).$$

When $a < 0$, similar WENO procedures can be applied. Below, we provide main formulas that are different from the case of $a \geq 0$, as needed for implementation purpose. Let $\xi = \frac{|a|\Delta t}{\Delta x}$,

$$\mathcal{H}^{(1)}(x_{i+\frac{1}{2}}) = -\Delta x \left((\frac{1}{6}\xi^3 - \frac{1}{6}\xi)u_{i-1}^n + (-\frac{1}{3}\xi^3 - \frac{1}{2}\xi^2 + \frac{5}{6}\xi)u_i^n + (\frac{1}{6}\xi^3 + \frac{1}{2}\xi^2 + \frac{1}{3}\xi)u_{i+1}^n \right) \tag{3.36}$$

$$\mathcal{H}^{(2)}(x_{i+\frac{1}{2}}) = -\Delta x \left((\frac{1}{6}\xi^3 - \frac{1}{2}\xi^2 + \frac{1}{3}\xi)u_i^n + (-\frac{1}{3}\xi^3 + \frac{1}{2}\xi^2 + \frac{5}{6}\xi)u_{i+1}^n + (\frac{1}{6}\xi^3 - \frac{1}{6}\xi)u_{i+2}^n \right) \tag{3.37}$$

$$\mathcal{H}^{(3)}(x_{i+\frac{1}{2}}) = -\Delta x \left((\frac{1}{6}\xi^3 - \xi^2 + \frac{11}{6}\xi)u_{i+1}^n + (-\frac{1}{3}\xi^3 + \frac{3}{2}\xi^2 - \frac{7}{6}\xi)u_{i+2}^n + (\frac{1}{6}\xi^3 - \frac{1}{2}\xi^2 + \frac{1}{3}\xi)u_{i+3}^n \right) \tag{3.38}$$

$$\gamma_1 = \frac{3}{10} - \frac{1}{4}\xi + \frac{1}{20}\xi^2, \quad \gamma_2 = \frac{3}{5} + \frac{1}{10}\xi - \frac{1}{10}\xi^2, \quad \gamma_3 = \frac{1}{10} + \frac{3}{20}\xi + \frac{1}{20}\xi^2$$

$$\begin{aligned}
\beta_1 &= \frac{13}{12}(u_{i-1}^n - 2u_i^n + u_{i+1}^n)^2 + \frac{1}{4}(u_{i-1}^n - 4u_i^n + 3u_{i+1}^n)^2, \\
\beta_2 &= \frac{13}{12}(u_i^n - 2u_{i+1}^n + u_{i+2}^n)^2 + \frac{1}{4}(u_i^n - u_{i+2}^n)^2, \\
\beta_3 &= \frac{13}{12}(u_{i+1}^n - 2u_{i+2}^n + u_{i+3}^n)^2 + \frac{1}{4}(3u_{i+1}^n - 4u_{i+2}^n + u_{i+3}^n)^2.
\end{aligned}$$

3.3.3 Extra large time step evolution

One way of implementing extra large time step evolution is to shift the solution by whole grid points first, then use the scheme to advect the fractional remainder, if the advection equation has constant coefficient. Yet we will describe another equivalent implementation, which gives hint of applying the scheme to equations with variable coefficients in Section 4. Again, we assume $a \geq 0$. When the time step is larger than the CFL restriction, $\Delta t \geq a\Delta x$, then $x_i - x_i^\star > \Delta x$. Let $i^\star$ to be the index such that $x_i^\star \in (x_{i^\star-1}, x_{i^\star}]$ and $\xi = \frac{x_{i^\star} - x_i^\star}{\Delta x}$. Let us

for the moment work with linear reconstructions. From Step 2 in Section 3.1,

$$\begin{aligned}\bar{\mathcal{H}}_i &= \int_{x_i^\star}^{x_i} u(\xi, t^n) d\xi \\ &= \sum_{j=i^\star+1}^{i} \int_{x_{j-1}}^{x_j} u(\xi, t^n) d\xi + \int_{x_i^\star}^{x_{i^\star}} u(\xi, t^n) d\xi \\ &= \sum_{j=i^\star+1}^{i} \mathcal{R}_1[x_{j-1}, x_j](u_{j-p_1}, \cdots, u_{j+q_1}) + \mathcal{R}_1[x_i^\star, x_{i^\star}](u_{i^\star-p_1}, \cdots, u_{i^\star+q_1}),\end{aligned}$$

where $\mathcal{R}_1[a, b]$ indicates the reconstruction of $\int_a^b u(\xi, t) d\xi$. If the operator $\mathcal{R}_1$ in the above equation is combined with $\mathcal{R}_2$ in equation (3.11) with a compact stencil as in the previous subsections, then

$$\mathcal{H}(x_{i+\frac{1}{2}}) = \sum_{j=i^\star+1}^{i} \mathcal{R}_2 \circ \mathcal{R}_1[x_{j-1}, x_j](u_{j-p}, \cdots, u_{j+q}) + \mathcal{R}_2 \circ \mathcal{R}_1[x_i^\star, x_{i^\star}](u_{i^\star-p}, \cdots, u_{i^\star+q}) \tag{3.39}$$

$$= \sum_{j=i^\star+1}^{i} \Delta x u_j^n + \mathcal{R}(u_{i^\star-p}, \cdots, u_{i^\star+q}), \tag{3.40}$$

where $\mathcal{R} = \mathcal{R}_2 \circ \mathcal{R}_1$ is a reconstruction procedure with compact reconstruction stencil as in equation (3.17). Equality (3.39) is true since $\mathcal{R}_2$ is a linear operator, and equality (3.40) is due to Proposition 3.7. Plugging these flux functions into equation (3.5) gives the scheme

$$\begin{aligned}u_i^{n+1} &= u_i^n - \frac{1}{\Delta x}\left((\sum_{j=i^\star+1}^{i} u_j^n \Delta x + \mathcal{R}(u_{i^\star-p}, \cdots, u_{i^\star+q})) - (\sum_{j=i^\star}^{i-1} u_j^n \Delta x + \mathcal{R}(u_{i^\star-1-p}, \cdots, u_{i^\star-1+q}) \right) \\ &= u_i^n - \frac{1}{\Delta x}\left(\Delta x(u_i^n - u_{i^\star}^n) + (\mathcal{R}(u_{i^\star-p}, \cdots, u_{i^\star+q}) - \mathcal{R}(u_{i^\star-1-p}, \cdots, u_{i^\star-1+q}))\right) \\ &= u_{i^\star}^n - \frac{1}{\Delta x}\left(\mathcal{R}(u_{i^\star-p}, \cdots, u_{i^\star+q}) - \mathcal{R}(u_{i^\star-1-p}, \cdots, u_{i^\star-1+q})\right). \end{aligned} \tag{3.41}$$

It is similar to the first order scheme, that although information is integrated along $x_i^\star$ to x_i to compute $\bar{\mathcal{H}}_i$, the final form of scheme (3.41) only involves the information around the foot of characteristics $x_i^\star$. When reconstructing $H(x_{i+\frac{1}{2}})$ in WENO fashion, we apply WENO mechanism only *locally* around $x_i^\star$, i.e. on the $\mathcal{R}$ in equation (3.41). Similar procedure is applied when $a < 0$.

3.3.4 Summarized procedure for equations with constant advection coefficient

A semi-Lagrangian scheme with $(2k+1)^{th}$ order WENO reconstruction for equations with constant advection coefficient is summarized below.

1. Locate the root of characteristics. Let $x_i^\star = x_i - a\Delta t, \quad i = 0, \cdots, N$, and $i^\star$ to be the index such that $x_i^\star \in (x_{i^\star-1}, x_{i^\star}]$.

2. - If $a \geq 0$, let $\xi = \frac{x_{i^\star} - x_i^\star}{\Delta x}$. Compute $H(x_{i+\frac{1}{2}})$ by

$$H(x_{i+\frac{1}{2}}) = \sum_{j=i^\star+1}^{i} u_j^n + H^\star(x_{i+\frac{1}{2}}), \tag{3.42}$$

   where $H^\star(x_{i+\frac{1}{2}})$ is reconstructed with $(2k+1)^{th}$ order WENO reconstruction from the stencil $\{u_{i^\star-k}, \cdots, u_{i^\star+k}\}$. Specifically, explicit formulas are given in Section 3.3.2 when $k = 1$ and $k = 2$, corresponding to third and fifth order WENO reconstructions.

   - If $a < 0$, let $\xi = \frac{x_i^\star - x_{i^\star-1}}{\Delta x}$. Compute $H(x_{i+\frac{1}{2}})$ by

$$H(x_{i+\frac{1}{2}}) = -\sum_{j=i+1}^{i^\star-1} u_j^n + H^\star(x_{i+\frac{1}{2}}), \tag{3.43}$$

   where $H^\star(x_{i+\frac{1}{2}})$ is reconstructed with $(2k+1)^{th}$ order WENO reconstruction from the stencil $\{u_{i^\star-k+1}, \cdots, u_{i^\star+k+1}\}$. Specifically, explicit formulas are given in Section 3.3.2 for third and fifth order WENO reconstructions.

3. Update u_i^{n+1} by equation (3.5) with $H(x_{i\pm\frac{1}{2}})$ computed in the previous step.

4 For variable coefficients

In this section, we generalize the scheme in Section 3 to the equations with general variable coefficient $a(x,t)$,

$$u_t + (a(x,t)u)_x = 0. \tag{4.1}$$

We assume $a(x,t)$ is continuous with respect to x and t. In the PDE level, one of the key differences between equation (3.1) and (4.1) is the characteristics. The characteristics for equation (3.1) are parallel straight lines, and the solutions along characteristics are constant; whereas the characteristics for equation (4.1) are curves, and the solution along each characteristic is not always a constant. On the other hand, the conservation property of u is kept, i.e. $\frac{d}{dt}\int u(x,t)dx = 0$. Scheme-wise, the basic formulation of the first order semi-Lagrangian

finite difference scheme approximating the conservative equation (4.1) would be similar as that for equation (3.1). However, there are additional numerical implementation issues. For example, the tracing back of curvy characteristics can no longer be carried out analytically; rather a numerical procedure has to be involved to solve

$$\frac{dX(t)}{dt} = a(X(t), t), \quad \text{with} \quad X(t^{n+1}) = x_i, \tag{4.2}$$

back to $X(t^n) = x_i^\star$ with a high order time integrator. In our implementation in Section 5, a fourth order Runge-Kutta method is applied in a single time step, or with multiple time steps with step size small enough to guarantee stability and accuracy of locating $x_i^\star$. The major difficulty, however, lies in the implementation of high (higher than first) order reconstruction operators $\mathcal{R}_1$, $\mathcal{R}_2$ in equations (3.10), (3.11) or the combination of them $\mathcal{R}$ in equation (3.17). We address this difficulty in Section 4.1 below. The algorithm is summarized in Section 4.2.

4.1 ENO/WENO reconstructions for equations with variable coefficients

We first discuss high order ENO/WENO reconstructions for small time step evolution when $|x_i^\star - x_i| \le \Delta x$ for all i. Generalization of the scheme for extra large time step evolution follows similar fashion as in Section 3.3.3.

Assuming $|x_i^\star - x_i| \le \Delta x$ for all i, we would like to reconstruct the numerical flux with high order in ENO fashion. For a k^{th} order reconstruction, the ENO selection algorithm picks a k-point stencil among k candidate stencils, according to the smoothness of the stencil measured by Newton divided difference. Below, we apply the ENO idea in our second and third order reconstructions. We refer the readers to [15, 9] for more details.

Second order ENO reconstructions.

1. If $x_i^\star \le x_i$, then we start with a one-point stencil $\{u_i\}$. Let $\xi_j = \frac{x_j - x_j^\star}{\Delta x}$, $j = i-1, i, i+1$.

   - If $|x_i - x_{i-1}| \le |x_i - x_{i+1}|$, then take $\{u_{i-1}, u_i\}$ as reconstruction stencil to reconstruct $\bar{\mathcal{H}}_{i-1}$ and $\bar{\mathcal{H}}_i$, which is then used to reconstruct $\mathcal{H}(x_{i+\frac{1}{2}})$.

$$\mathcal{H}(x_{i+\frac{1}{2}}) = \Delta x \left((-\frac{1}{2}\xi_{-1} - \frac{1}{4}\xi_{-1}^2 + \frac{3}{4}\xi_0^2)u_{i-1}^n + (\frac{1}{4}\xi_{-1}^2 - \frac{3}{4}\xi_0^2 + \frac{3}{2}\xi_0)u_i^n \right). \tag{4.3}$$

- If $|x_i - x_{i-1}| > |x_i - x_{i+1}|$, then take $\{u_i, u_{i+1}\}$ as reconstruction stencil to reconstruct $\bar{\mathcal{H}}_i$ and $\bar{\mathcal{H}}_{i+1}$, which is then used to reconstruct $\mathcal{H}(x_{i+\frac{1}{2}})$.

$$\mathcal{H}(x_{i+\frac{1}{2}}) = \Delta x \left((\frac{1}{2}\xi_0 + \frac{1}{4}\xi_0^2 + \frac{1}{4}\xi_1^2)u_i^n + (-\frac{1}{4}\xi_0^2 + \frac{1}{2}\xi_1 - \frac{1}{4}\xi_1^2)u_{i+1}^n \right). \tag{4.4}$$

2. If $x_i^\star > x_i$, then we start with a one-point stencil $\{u_{i+1}\}$. Let $\xi_j = \frac{x_j^\star - x_j}{\Delta x}$, $j = i, i+1, i+2$.

- If $|x_i - x_{i+1}| \le |x_{i+2} - x_{i+1}|$, then take $\{u_i, u_{i+1}\}$ as reconstruction stencil to reconstruct $\bar{\mathcal{H}}_{i-1}$ and $\bar{\mathcal{H}}_i$, which is then used to reconstruct $\mathcal{H}(x_{i+\frac{1}{2}})$.

$$\mathcal{H}(x_{i+\frac{1}{2}}) = \Delta x \left((\xi_{-1} - \frac{1}{4}\xi_{-1}^2 + \frac{3}{4}\xi_0^2 - \frac{3}{2}\xi_0)u_i^n + (-\frac{1}{2}\xi_{-1} + \frac{1}{4}\xi_{-1}^2 - \frac{3}{4}\xi_0^2)u_{i+1}^n \right). \tag{4.5}$$

- If $|x_i - x_{i+1}| > |x_{i+2} - x_{i+1}|$ then take $\{u_{i+1}, u_{i+2}\}$ as reconstruction stencil to reconstruct $\bar{\mathcal{H}}_i$ and $\bar{\mathcal{H}}_{i+1}$, which is then used to reconstruct $\mathcal{H}(x_{i+\frac{1}{2}})$.

$$\mathcal{H}(x_{i+\frac{1}{2}}) = \Delta x \left((-\xi_0 + \frac{1}{4}\xi_0^2 - \frac{1}{2}\xi_1 + \frac{1}{4}\xi_1^2)u_{i+1}^n + (\frac{1}{2}\xi_0 - \frac{1}{4}\xi_0^2 - \frac{1}{4}\xi_1^2)u_{i+2}^n \right). \tag{4.6}$$

Third order ENO reconstructions. Similar to the second order case, we apply the ENO idea directly to our reconstruction. We omit the details of ENO selection algorithm, but refer the readers to [15, 9].

1. If $x_i^\star \le x_i$, then we start with a one-point stencil $\{u_i\}$. We apply the ENO selection algorithm, which picks the smoothest stencil of the three three-point stencils

$$S_1 = \{u_{i-2}, u_{i-1}, u_i\}, \quad S_2 = \{u_{i-1}, u_i, u_{i+1}\}, \quad S_3 = \{u_i, u_{i+1}, u_{i+2}\},$$

according to the smoothness of the stencil measured by Newton divided difference. Let $\xi_j = \frac{x_j - x_j^\star}{\Delta x}$, $j = i-2, \cdots, i+2$. The reconstructions of flux function $\mathcal{H}(x_{i+\frac{1}{2}})$ from S_1, S_2 and S_3 are given respectively by

$$\begin{aligned}\mathcal{H}(x_{i+\frac{1}{2}}) = \Delta x \Big(& (\frac{1}{3}\xi_{-2} + \frac{1}{4}\xi_{-2}^2 + \frac{1}{18}\xi_{-2}^3 - \frac{7}{24}\xi_{-1}^2 - \frac{7}{36}\xi_{-1}^3 - \frac{11}{24}\xi_0^2 + \frac{11}{36}\xi_0^3)u_{i-2}^n \\ & + (-\frac{1}{3}\xi_{-2}^2 - \frac{1}{9}\xi_{-2}^3 - \frac{7}{6}\xi_{-1} + \frac{7}{18}\xi_{-1}^3 + \frac{11}{6}\xi_0^2 - \frac{11}{18}\xi_0^3)u_{i-1}^n \\ & + (\frac{1}{12}\xi_{-2}^2 + \frac{1}{18}\xi_{-2}^3 + \frac{7}{24}\xi_{-1}^2 - \frac{7}{36}\xi_{-1}^3 + \frac{11}{6}\xi_0 - \frac{11}{8}\xi_0^2 + \frac{11}{36}\xi_0^3)u_i^n \Big)\end{aligned} \tag{4.7}$$

$$\mathcal{H}(x_{i+\frac{1}{2}}) = \Delta x \Big((-\frac{1}{6}\xi_{-1} - \frac{1}{8}\xi_{-1}^2 - \frac{1}{36}\xi_{-1}^3 + \frac{5}{24}\xi_0^2 + \frac{5}{36}\xi_0^3 - \frac{1}{12}\xi_1^2 + \frac{1}{18}\xi_1^3)u_{i-1}^n$$
$$+ (\frac{1}{6}\xi_{-1}^2 + \frac{1}{18}\xi_{-1}^3 + \frac{5}{6}\xi_0 - \frac{5}{18}\xi_0^3 + \frac{1}{3}\xi_1^2 - \frac{1}{9}\xi_1^3)u_i^n$$
$$+ (-\frac{1}{24}\xi_{-1}^2 - \frac{1}{36}\xi_{-1}^3 - \frac{5}{24}\xi_0^2 + \frac{5}{36}\xi_0^3 + \frac{1}{3}\xi_1 - \frac{1}{4}\xi_1^2 + \frac{1}{18}\xi_1^3)u_{i+1}^n \Big) \tag{4.8}$$

$$\mathcal{H}(x_{i+\frac{1}{2}}) = \Delta x \Big((\frac{1}{3}\xi_0 + \frac{1}{4}\xi_0^2 + \frac{1}{18}\xi_0^3 + \frac{5}{24}\xi_1^2 + \frac{5}{36}\xi_1^3 + \frac{1}{24}\xi_2^2 - \frac{1}{36}\xi_2^3)u_i^n$$
$$+ (-\frac{1}{3}\xi_0^2 - \frac{1}{9}\xi_0^3 + \frac{5}{6}\xi_1 - \frac{5}{18}\xi_1^3 - \frac{1}{6}\xi_2^2 + \frac{1}{18}\xi_2^3)u_{i+1}^n$$
$$+ (\frac{1}{12}\xi_0^2 + \frac{1}{18}\xi_0^3 - \frac{5}{24}\xi_1^2 + \frac{5}{36}\xi_1^3 - \frac{1}{6}\xi_2 + \frac{1}{8}\xi_2^2 - \frac{1}{36}\xi_2^3)u_{i+2}^n \Big). \tag{4.9}$$

2. If $x_i^\star > x_i$, then we start with a one-point stencil $\{u_{i+1}\}$. We pick the smoothest stencil of the three three-point stencils

$$S_1 = \{u_{i-1}, u_i, u_{i+1}\}, \quad S_2 = \{u_i, u_{i+1}, u_{i+2}\}, \quad S_3 = \{u_{i+1}, u_{i+2}, u_{i+3}\},$$

in ENO fashion. Let $\xi_j = \frac{x_j^\star - x_j}{\Delta x}$, $j = i-1, \cdots, i+3$. The reconstructions of flux function $\mathcal{H}(x_{i+\frac{1}{2}})$ from S_1, S_2 and S_3 are given respectively by

$$\mathcal{H}(x_{i+\frac{1}{2}}) = \Delta x \Big((-\xi_{-2} + \frac{5}{12}\xi_{-2}^2 - \frac{1}{18}\xi_{-2}^3 + \frac{7}{6}\xi_{-1} - \frac{7}{8}\xi_{-1}^2 + \frac{7}{36}\xi_{-1}^3 + \frac{11}{24}\xi_0^2 - \frac{11}{36}\xi_0^3)u_{i-1}^n$$
$$+ (\xi_{-2} - \frac{2}{3}\xi_{-2}^2 + \frac{1}{9}\xi_{-2}^3 + \frac{7}{6}\xi_{-1}^2 - \frac{7}{18}\xi_{-1}^3 - \frac{11}{6}\xi_0 + \frac{11}{18}\xi_0^3)u_i^n$$
$$+ (-\frac{1}{3}\xi_{-2} + \frac{1}{4}\xi_{-2}^2 - \frac{1}{18}\xi_{-2}^3 - \frac{7}{24}\xi_{-1}^2 + \frac{7}{36}\xi_{-1}^3 - \frac{11}{24}\xi_0^2 - \frac{11}{36}\xi_0^3)u_{i+1}^n \Big) \tag{4.10}$$

$$\mathcal{H}(x_{i+\frac{1}{2}}) = -\Delta x \Big((-\frac{1}{2}\xi_{-1} + \frac{5}{24}\xi_{-1}^2 - \frac{1}{36}\xi_{-1}^3 + \frac{5}{6}\xi_0 - \frac{5}{8}\xi_0^2 + \frac{5}{36}\xi_0^3 - \frac{1}{12}\xi_1^2 + \frac{1}{18}\xi_1^3)u_i^n$$
$$- (\frac{1}{2}\xi_{-1} - \frac{1}{3}\xi_{-1}^2 + \frac{1}{18}\xi_{-1}^3 + \frac{5}{6}\xi_0^2 - \frac{5}{18}\xi_0^3 + \frac{1}{3}\xi_1 - \frac{1}{9}\xi_1^3)u_{i+1}^n$$
$$- (-\frac{1}{6}\xi_{-1} + \frac{1}{8}\xi_{-1}^2 - \frac{1}{36}\xi_{-1}^3 - \frac{5}{24}\xi_0^2 + \frac{5}{36}\xi_0^3 + \frac{1}{12}\xi_1^2 + \frac{1}{18}\xi_1^3)u_{i+2}^n \Big) \tag{4.11}$$

$$\mathcal{H}(x_{i+\frac{1}{2}}) = -\Delta x \Big((\xi_0 - \frac{5}{12}\xi_0^2 + \frac{1}{18}\xi_0^3 + \frac{5}{6}\xi_1 - \frac{5}{8}\xi_1^2 + \frac{5}{36}\xi_1^3 + \frac{1}{24}\xi_2^2 - \frac{1}{36}\xi_2^3)u_{i+1}^n$$
$$- (-\xi_0 + \frac{2}{3}\xi_0^2 - \frac{1}{9}\xi_0^3 + \frac{5}{6}\xi_1^2 - \frac{5}{18}\xi_1^3 - \frac{1}{6}\xi_2 + \frac{1}{18}\xi_2^3)u_{i+2}^n$$
$$- (\frac{1}{3}\xi_0 - \frac{1}{4}\xi_0^2 + \frac{1}{18}\xi_0^3 - \frac{5}{24}\xi_1^2 + \frac{5}{36}\xi_1^3 - \frac{1}{24}\xi_2^2 - \frac{1}{36}\xi_2^3)u_{i+3}^n \Big). \tag{4.12}$$

Remark 4.1. The ξ_j's in the ENO reconstruction can be of different signs, for example around the point where $a(x,t)$ changes sign. The reconstruction formulas provided above accommodates that situation.

Remark 4.2. When taking $\xi = \xi_j$, $j = -1, \cdots, 1$, equation (4.3)-(4.4) (or (4.5)-(4.6)) will be reduced to equation (3.27)-(3.28) (or (3.31)-(3.32)). Similarly, when taking $\xi = \xi_j$, $j = -2, \cdots, 2$, equation (4.7)-(4.9) (or (4.10)-(4.12)) will be reduced to equation (3.33)-(3.35) (or (3.36)-(3.38)).

Remark 4.3. There do not always exist linear weights γ_1 and γ_2, such that $\mathcal{H}(x_{i+\frac{1}{2}})$ reconstructed in equation (4.8) from a three point stencil $\{u_{i-1}, u_i, u_{i+1}\}$, is a linear combination of $\mathcal{H}(x_{i+\frac{1}{2}})$ reconstructed in equation (4.3) and (4.4) from two two-point stencils $\{u_{i-1}, u_i\}$ and $\{u_i, u_{i+1}\}$. For example, if consider $\xi_{-1} = \xi_0 = 0$ and $\xi_1 = 1$, then equation (4.3), (4.4) and (4.8) becomes respectively

$$\begin{aligned}
\mathcal{H}(x_{i+\frac{1}{2}}) &= 0 \cdot u_{i-1}^n + 0 \cdot u_i^n \\
\mathcal{H}(x_{i+\frac{1}{2}}) &= \frac{1}{4}u_i^n + \frac{1}{4}u_{i+1}^n \\
\mathcal{H}(x_{i+\frac{1}{2}}) &= -\frac{1}{36}u_{i-1}^n + \frac{2}{9}u_i^n - \frac{1}{36}u_{i+1}^n,
\end{aligned}$$

in which case the linear weights γ_1 and γ_2 do not exist.

Remark 4.4. Although there might not always exist linear weights γ_i, $i = 1, \cdots, k$ which gives a high order ($(2k-1)^{th}$ order) reconstruction, it is still possible to design a WENO reconstruction, which is often more robust in high order accuracy than ENO reconstruction, by choosing specific linear weights without the consideration of improving accuracy over that of individual small stencils. Specifically, we have applied second order WENO reconstruction with linear weights $\frac{1}{2}$, $\frac{1}{2}$, and third order WENO reconstruction with linear weights $\frac{1}{6}$, $\frac{2}{3}$ and $\frac{1}{6}$, in our numerical experiments. These linear weights are chosen empirically according to the performances of schemes in test problems in the next section. With the linear weights specified, the WENO reconstruction procedures follow similar fashion with those in Section 3.3.2. We omit the details for brevity.

Remark 4.5. Similar procedure as in Section 3.3.3 can be applied to deal with extra large time step evolution.

4.2 Summarized procedure for equations with variable coefficient

A semi-Lagrangian scheme with k^{th} order ENO/WENO reconstruction is summarized below.

1. Locate the root of characteristic from x_i at t^{n+1} back to $x_i^\star$ at t^n. A high order numerical integrator such as fourth order Runge-Kutta method can be applied to locate $x_i^\star$.

2. - If $x_i^\star \le x_i$. Let $i^\star$ be the index such that $x_i^\star \in [x_{i^\star-1}, x_{i^\star}]$. Compute $H(x_{i+\frac{1}{2}})$ by equation (3.42) with $H^\star(x_{i+\frac{1}{2}})$ reconstructed with k^{th} order ENO/WENO reconstruction from the stencil $\{u_{i^\star-k}, \cdots, u_{i^\star+k}\}$. Specifically, explicit formulas are given in Section 4.1 when $k = 1$ and $k = 2$, corresponding to second and third order ENO/WENO reconstructions.

   - If $x_i^\star > x_i$. Let $i^\star$ be the index such that $x_i^\star \in [x_{i^\star-1}, x_{i^\star}]$. Compute $H(x_{i+\frac{1}{2}})$ by equation (3.43) with $H^\star(x_{i+\frac{1}{2}})$ reconstructed with k^{th} order ENO/WENO reconstruction from the stencil $\{u_{i^\star-k+1}, \cdots, u_{i^\star+k+1}\}$. Specifically, explicit formulas are given in Section 4.1 for second and third order ENO/WENO reconstructions.

3. Update u_i^{n+1} by equation (3.5) with $H(x_{i\pm\frac{1}{2}})$ computed in the previous step.

5 Numerical tests

In this section, the proposed semi-Lagrangian finite difference schemes with various WENO or ENO reconstructions are tested on linear advection, rigid body rotation and swirling deformation.

Example 5.1. (one dimensional linear translation)

$$u_t + u_x = 0, \quad x \in [0, 2\pi]. \tag{5.1}$$

The proposed semi-Lagrangian finite difference methods with various WENO/ENO reconstructions are used to solve equation (5.1) with smooth initial data $u(x, 0) = \sin(x)$ and exact solution $u(x, t) = \sin(x - t)$. Table 5.1 gives the L^1 error and the corresponding order of convergence for schemes with third order and fifth order WENO reconstruction, denoted as WENO3 and WENO5. Table 5.2 gives the corresponding results for schemes with second and third order ENO reconstructions, denoted as ENO2 and ENO3, and with second

order WENO reconstruction with linear weights $\frac{1}{2}$, $\frac{1}{2}$ denoted as WENO2, and with third order WENO reconstruction with linear weights $\frac{1}{6}$, $\frac{2}{3}$ and $\frac{1}{6}$, denoted as WENO3 (2). The linear weights here are chosen empirically according to the performances of schemes in test problems in this paper. Expected order of convergence is observed for all reconstruction operators. For scheme with WENO3 reconstruction, only second order convergence is observed as in the regular third order WENO reconstruction. The schemes also inherit the essentially non-oscillatory property of WENO/ENO reconstructions, when advecting rectangular waves. Numerical results are omitted here to save space. Figure 5.1 is the plot of L^1 error versus the $CFL = \frac{\Delta t}{\Delta x}$ with WENO3 and WENO5, and with ENO2 and WENO2 reconstructions. Two observations can be concluded from the Figure: (1) the error from spatial reconstruction takes peak when ξ, the fractional remainder, is around $\frac{1}{2}$; and the error is at the machine precision when $\xi = 0$, corresponding to exact shifting of grid points; (2) the error follows a decreasing trend, as CFL increases. The more number of time steps (the smaller time step) the scheme evolved with, the larger the error will be. The plots for schemes with ENO3 and WENO3(2) reconstructions are similar, thus omitted to save space.

Table 5.1: Order of accuracy for (5.1) with $u(x, t = 0) = \sin(x)$ at $T = 20$. $CFL = 2.2$.

–	WENO3		WENO5	
mesh	error	order	error	order
40	1.03E-2	–	1.18E-5	–
80	2.66E-3	1.96	3.63E-7	5.03
120	1.16E-3	2.04	4.74E-8	5.02
160	6.52E-4	2.02	1.12E-8	5.02
200	4.11E-4	2.07	3.67E-9	4.99

Example 5.2. (one dimensional equation with variable coefficient)

$$u_t + (\sin(x)u)_x = 0 \quad x \in [0, 2\pi]. \tag{5.2}$$

The initial condition is $u(x, 0) = 1$ and the boundary condition is periodic. The exact solution is

$$u(x, t) = \frac{\sin\left(2\tan^{-1}(e^{-T}\tan(\frac{x}{2}))\right)}{\sin(x)}.$$

Table 5.2: Order of accuracy for (5.1) with $u(x, t = 0) = \sin(x)$ at $T = 20$. $CFL = 2.2$.

–	ENO2		ENO3		WENO2		WENO3(2)	
mesh	error	order	error	order	error	order	error	order
40	1.16E-2	–	3.19E-4	–	1.07E-2	–	3.58E-5	–
80	3.31E-3	1.81	4.06E-5	2.97	2.79E-3	1.94	3.42E-6	3.39
120	1.55E-3	1.87	1.20E-5	3.00	1.23E-3	2.01	9.46E-7	3.17
160	8.94E-4	1.91	5.05E-6	3.02	6.86E-4	2.04	3.86E-7	3.12
200	5.87E-4	1.89	2.59E-6	2.99	4.38E-4	2.01	1.96E-7	3.04

The proposed schemes with first order reconstruction, as well as ENO2, WENO2, ENO3, WENO3(2) reconstructions are applied to solve equation (5.2). Tables 5.3, 5.4 and 5.5 give the L^1, L^∞ error and the corresponding order of convergence for those schemes with $CFL = 3$ at $T = 1$. Expected first order accuracy is observed in both L^1 and L^∞ norm in Table 5.3. In Table 5.4, the order of convergence for scheme with ENO2 reconstruction is slightly less than expected (second order) in both L^1 and L^∞ norm. The magnitude of error has been greatly reduced when WENO2 reconstruction is applied; and second order convergence is observed. Similarly, in Table 5.5, the order of convergence for scheme with ENO3 reconstruction is less than expected (third order) in both L^1 and L^∞ norm. The magnitude of error has been greatly reduced when WENO3(2) reconstruction is applied; and around fourth order convergence is observed in this test. Figure 5.2 is the plot of L^1 error versus the $CFL = \frac{\Delta t}{\Delta x}$ for schemes with ENO2 (left) and WENO2 (right) reconstructions. It is observed that, the error oscillates as a function of CFL, which partially explains why the order of convergence for ENO2 in Table 5.4 is not very clean. With the WENO reconstruction, not only the magnitude of the error has been greatly reduced, but also clean second order convergence is observed.

Example 5.3. (two dimensional linear transport)

$$u_t + u_x + u_y = 0, \quad x \in [0, 2\pi], \quad y \in [0, 2\pi]. \tag{5.3}$$

The equation is being split into two one-dimensional equations, each of which is evolved by the proposed semi-Lagrangian finite difference method. For any 2-D linear transport equation, the semi-Lagrangian method is essentially a shifting procedure. Since the x-shifting and

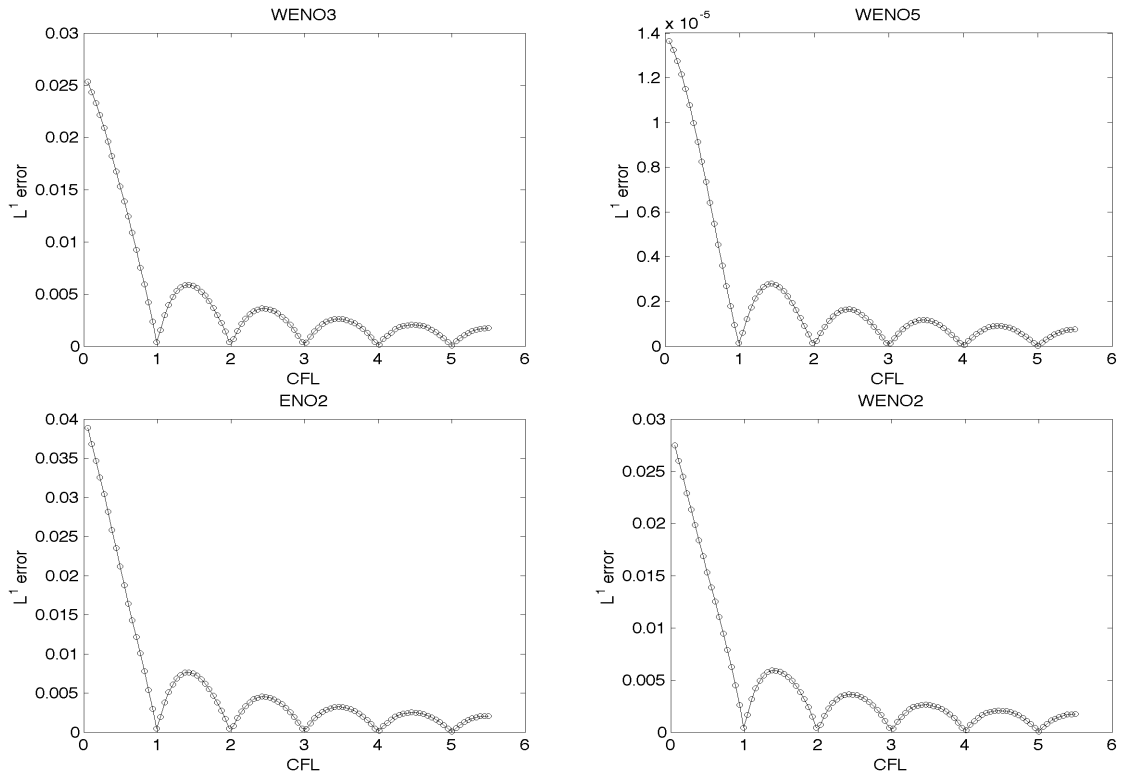

Figure 5.1: Plots of error versus the CFL number with various reconstructions as indicated at the top of each plot. The mesh is $N = 80$.

y-shifting operators commute, there is no dimensional splitting error in time and the spatial error is the dominant error. Table 5.6 gives the L^1 error and the corresponding order of convergence when schemes with WENO3 and WENO5 reconstructions are applied to equation (5.3) with smooth solution $u(x, y, t) = \sin(x + y - 2t)$. Again second order convergence is observed for WENO3 reconstruction, and very clean fifth order convergence is observed for WENO5 reconstruction as expected. Table 5.7 gives the L^1 error and the corresponding order of convergence when schemes with ENO2, WENO2, ENO3, WENO3(2) reconstructions are applied to the same problem. Roughly second and third order convergence are observed from schemes with ENO2 and ENO3 reconstructions; smaller error, as well as clean second and third order convergence are observed from schemes with WENO2 and WENO3(2) reconstructions. Figure 5.3 gives the numerical solutions of advecting a 2-D cross shape. As anticipated when using ENO/WENO reconstructions, non-oscillatory numerical capturing of the discontinuities is observed. In our 2-D simulation, $CFL = \frac{\Delta t}{\Delta x} + \frac{\Delta t}{\Delta y}$.

Table 5.3: First order scheme for (5.2) with $u(x, t = 0) = 1$ at $T = 1$ with $CFL = 3$.

–	L^1 error		L^∞ error	
mesh	error	order	error	order
40	5.83E-2	–	0.17	–
80	2.93E-2	0.99	8.80E-2	0.94
160	1.47E-2	1.00	4.46E-2	0.98
320	7.34E-3	1.00	2.23E-2	0.94
640	3.67E-3	1.00	1.16E-2	1.00

Table 5.4: Schemes with ENO2 and WENO2 reconstructions for (5.2) with $u(x, t = 0) = 1$ at $T = 1$ with $CFL = 3$.

–	ENO2				WENO2			
–	L^1 error		L^∞ error		L^1 error		L^∞ error	
mesh	error	order	error	order	error	order	error	order
40	9.83E-3	–	8.98E-2	–	3.81E-3	–	2.47E-2	–
80	3.99E-3	1.30	3.25E-2	1.47	9.20E-4	2.05	7.68E-3	1.69
160	1.17E-3	1.77	2.10E-2	0.62	2.06E-4	2.16	1.95E-3	1.98
320	5.38E-4	1.12	7.56E-3	1.48	4.77E-5	2.11	5.26E-4	1.89
640	1.60E-4	1.75	2.08E-3	1.86	1.14E-5	2.06	1.42E-4	1.88

Example 5.4. (rigid body rotation)

$$u_t - (yu)_x + (xu)_y = 0, \quad x \in [-\pi, \pi], \quad y \in [-\pi, \pi]. \tag{5.4}$$

The equation is being Strang split into two one-dimensional equations, each of which is evolved by the proposed semi-Lagrangian finite difference method. The initial condition we used is plotted in Figure 5.4 in both mesh and contour plots. It includes a slotted disk, a cone as well as a smooth hump, similar to the one in [19] for comparison purpose. The numerical solutions after six full revolutions from schemes with WENO3, WENO5, ENO2, WENO2, ENO3 and WENO3(2) reconstruction operators are plotted in Figure 5.5 by mesh and in Figure 5.6 by slides benchmarked with exact solution. With all reconstructions, non-oscillatory capturing of discontinuities is observed. However, schemes with high order reconstruction, such as WENO5 and WENO3(2), are observed to be less dissipative, therefore outperform schemes with lower order reconstructions.

Table 5.5: Schemes with ENO3 and WENO3 (2) reconstructions for (5.2) with $u(x, t = 0) = 1$ at $T = 1$ with $CFL = 3$.

–	ENO3				WENO3			
–	L^1 error		L^∞ error		L^1 error		L^∞ error	
mesh	error	order	error	order	error	order	error	order
40	2.26E-3	–	2.55E-2	–	4.61E-4	–	4.63E-3	–
80	4.95E-4	2.19	6.41E-3	1.99	2.65E-5	4.12	5.82E-4	2.99
160	9.28E-5	2.42	1.54E-3	2.05	1.27E-6	4.37	4.62E-5	3.66
320	2.50E-5	1.89	4.28E-4	1.85	5.89E-8	4.44	3.08E-6	3.91
640	4.25E-6	2.56	1.13E-4	1.92	4.13E-9	3.83	1.78E-7	4.11

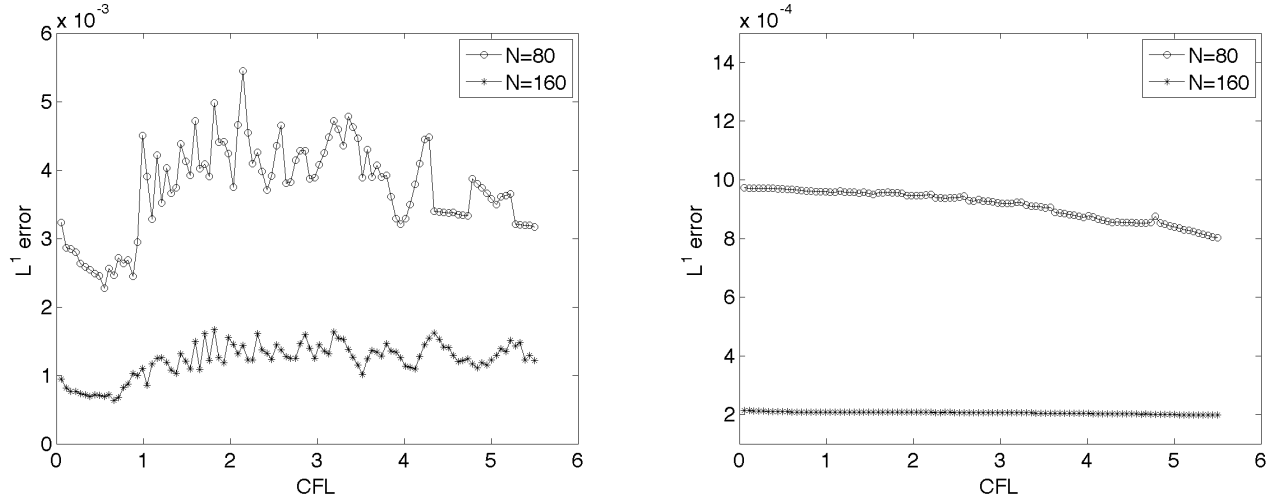

Figure 5.2: Plots of error versus the CFL number with the mesh $N = 80$ and $N = 160$ for schemes with ENO2 (left) and WENO2 (right) reconstructions.

Example 5.5. (Swirling deformation flow) We use the test case in [19] with similar parameters to allow a direct comparison. We consider solving

$$u_t - (\cos^2(\frac{x}{2})\sin(y)g(t)u)_x + (\sin(x)\cos^2(\frac{y}{2})g(t)u)_y = 0, \quad x \in [-\pi, \pi], \quad y \in [-\pi, \pi], \tag{5.5}$$

with $g(t) = \cos(\pi t/T)\pi$. In our test case, we use the same set of initial condition as in Example 5.4, which is quite challenging. We choose $T = 1.5$ and numerically integrate the solution up to time 0.75, when the initial profile is greatly deformed, and to time 1.5, when the initial profile is recovered. Figure 5.7 shows numerical results (in both mesh and contour plots) from the scheme with ENO2 reconstruction with first order Strang splitting with $CFL = 2$ and $CFL = 1$, and with second order Strang splitting with $CFL = 1$, when the

Table 5.6: Order of accuracy for solving (5.3) with $u(x, y, t = 0) = \sin(x + y)$ at $T = 20$. $CFL = 2.2$.

–	WENO3		WENO5	
mesh	error	order	error	order
20×20	0.14	–	2.78E-3	–
40×40	6.28E-2	1.16	8.75E-5	4.98
60×60	2.86E-2	1.94	1.15E-5	5.00
80×80	1.60E-2	2.01	2.73E-6	5.00

Table 5.7: Order of accuracy for (5.3) with $u(x, y, t = 0) = \sin(x+y)$ at $T = 20$. $CFL = 2.2$.

–	ENO2		WENO2		ENO3		WENO3(2)	
mesh	error	order	error	order	error	order	error	order
20×20	0.16	–	0.14	–	1.91E-2	–	4.57E-3	–
40×40	6.36E-2	1.31	6.26E-2	1.16	2.43E-3	2.97	3.29E-4	3.80
60×60	3.81E-2	1.25	2.86E-2	1.93	7.21E-4	3.00	8.35E-5	3.38
80×80	2.23E-2	1.86	1.60E-2	2.02	3.04E-4	3.00	3.32E-5	3.21

initial profile should be recovered. The splitting error is quite significant for the first order splitting scheme with $CFL = 2$. The solution approximates the initial profile well when the second order Strang splitting is applied with $CFL = 1$, which has relatively small dimensional splitting error. Numerical solutions from schemes with second order Strang splitting with $CFL = 1$ and ENO2, WENO2, ENO3 and WENO3(2) reconstruction operators are plotted in Figure 5.8 in mesh and contour plots and in Figure 5.9 by slides benchmarked with the exact solution. Decent results are obtained for all reconstructions. Schemes with ENO3 and WENO3(2) reconstructions are observed to outperform the schemes with ENO2 and WENO2 reconstructions. Figure 5.10 shows the mesh and contour plots of the numerical solution of the scheme with WENO3(2) reconstruction at the final integration time 0.75, when the solution is quite deformed.

Example 5.6. We numerically solve equation (5.5) with $g(t) = 1$ and the initial condition $u(x, y, t = 0) = 1$, if $\sqrt{(x-\pi)^2 + (y-\pi)^2} \leq \frac{8\pi}{5}$; and $u(x, y, t = 0) = 0$ otherwise. The test case here is also considered in [19]. The numerical solutions at $T = 2.5$ of schemes with ENO3 and WENO3 (2) reconstructions are plotted in Figure 5.11. The results from

schemes with ENO3 and WENO3 (2) reconstructions approximate the exact solution quiet well. They also outperform schemes with ENO2 and WENO2 reconstruction, whose plots are omitted to save space.

6 Conclusions

In this paper, we propose a semi-Lagrangian finite difference scheme for simulating advection in incompressible flows. Extensive numerical experiments, including the very challenging problem of rigid body rotation and swirling deformation, have been performed by applying the proposed semi-Lagrangian finite difference scheme with various reconstruction operators, such as WENO3, WENO5, ENO2, WENO2, ENO3, WENO3 (2). The proposed high order schemes have been shown to perform very well both by accuracy and by resolution of sharp interface. Future research directions include (1) developing truly multi-dimensional semi-Lagrangian finite difference scheme; (2) applications of algorithms developed in this paper to relativistic plasma applications.

References

[1] M. Begue, A. Ghizzo, P. Bertrand, E. Sonnendrucker, and O. Coulaud, *Two-dimensional semi-Lagrangian Vlasov simulations of laser–plasma interaction in the relativistic regime*, Journal of Plasma Physics, 62 (1999), pp. 367–388.

[2] N. Besse and E. Sonnendrucker, *Semi-Lagrangian schemes for the Vlasov equation on an unstructured mesh of phase space*, Journal of Computational Physics, 191 (2003), pp. 341–376.

[3] J. Carrillo and F. Vecil, *Nonoscillatory interpolation methods applied to Vlasov-based models*, SIAM Journal on Scientific Computing, 29 (2007), p. 1179.

[4] J. A. Carrillo, A. Majorana, and F. Vecil, *A semi-lagrangian deterministic solver for the semiconductor Boltzmann-Poisson system*, Communications in Computational Physics, (2007), pp. 1027–1054.

[5] J. A. Carrillo and F. Vecil, *Nonoscillatory Interpolation Methods Applied to Vlasov-Based Models*, SIAM Journal on Scientific Computing, 29 (2007), p. 1179.

[6] C. Cheng and G. Knorr, *Integration of the Vlasov equation in configuration space*, tech. rep., COO–2059-47, Iowa Univ., Iowa City (USA). Dept. of Physics and Astronomy, 1975.

[7] P. Childs and K. Morton, *Characteristic Galerkin methods for scalar conservation laws in one dimension*, SIAM Journal on Numerical Analysis, 27 (1990), pp. 553–594.

[8] A. Christlieb, M. Morton, and J.-M. Qiu, *Higher order dimensional splitting with integral deferred corrections with applications in Vlasov equation*, In preparation.

[9] B. Cockburn, C. Johnson, C.-W. Shu, and E. Tadmor, *Advanced numerical approximation of nonlinear hyperbolic equations*, Springer New York, 1998.

[10] P. Colella and P. Woodward, *The piecewise parabolic method(PPM) for gas-dynamical simulations*, Journal of computational physics, 54 (1984), pp. 174–201.

[11] N. Crouseilles, G. Latu, and E. Sonnendrucker, *Hermite spline interpolation on patches for parallelly solving the Vlasov-Poisson equation*, International Journal of Applied Mathematics and Computer Science, 17 (2007), pp. 335–349.

[12] F. Filbet and E. Sonnendrucker, *Comparison of eulerian Vlasov solvers*, Computer Physics Communications, 150 (2003), pp. 247–266.

[13] F. Filbet, E. Sonnendrucker, and P. Bertrand, *Conservative numerical schemes for the Vlasov equation*, Journal of Computational Physics, 172 (2001), pp. 166–187.

[14] S. Gottlieb, D. Ketcheson, and C. Shu, *High order strong stability preserving time discretizations*, Journal of Scientific Computing, 38 (2009), pp. 251–289.

[15] A. Harten, B. Engquist, S. Osher, and S. Chakravarthy, *Uniformly high order essentially non-oscillatory schemes, III*, Journal of Computational Physics, 71 (1987), pp. 231–303.

[16] F. Huot, A. Ghizzo, P. Bertrand, E. Sonnendrucker, and O. Coulaud, *Instability of the time splitting scheme for the one-dimensional and relativistic Vlasov–Maxwell system*, Journal of Computational Physics, 185 (2003), pp. 512–531.

[17] G.-S. Jiang and C.-W. Shu, *Efficient implementation of weighted ENO schemes*, Journal of Computational Physics, 126 (1996), pp. 202–228.

[18] T. Lee and C. Lin, *A characteristic Galerkin method for discrete Boltzmann equation*, Journal of Computational Physics, 171 (2001), pp. 336–356.

[19] R. LeVeque, *High-resolution conservative algorithms for advection in incompressible flow*, SIAM Journal on Numerical Analysis, (1996), pp. 627–665.

[20] X.-D. Liu, S. Osher, and T. Chan, *Weighted essentially non-oscillatory schemes*, Journal of Computational Physics, 115 (1994), pp. 200–212.

[21] J.-M. Qiu and A. Christlieb, *A Conservative high order semi-Lagrangian WENO method for the Vlasov Equation*, Journal of Computational Physics, (accepted).

[22] J. Shi, C. Hu, and C. Shu, *A technique of treating negative weights in WENO schemes*, Journal of Computational Physics, 175 (2002), pp. 108–127.

[23] C. Shu, *High order weighted essentially non-oscillatory schemes for convection dominated problems*, SIAM Review, 51 (2009), pp. 82–126.

[24] C. Shu and S. Osher, *Efficient implementation of essentially non-oscillatory shock-capturing schemes*, Journal of Computational Physics, 77 (1988), pp. 439–471.

[25] E. Sonnendrucker, J. Roche, P. Bertrand, and A. Ghizzo, *The semi-Lagrangian method for the numerical resolution of Vlasov equations.*

[26] A. Staniforth and J. Cote, *Semi-Lagrangian integration schemes for atmospheric modelsA review*, Monthly Weather Review, 119 (1991), pp. 2206–2223.

[27] H. Takewaki, A. Nishiguchi, and T. Yabe, *Cubic interpolated pseudo-particle method(CIP) for solving hyperbolic-type equations*, Journal of Computational Physics, 61 (1985), pp. 261–268.

[28] T. Umeda, M. Ashour-Abdalla, and D. Schriver, *Comparison of numerical interpolation schemes for one-dimensional electrostatic Vlasov code*, Journal of Plasma Physics, 72 (2006), pp. 1057–1060.

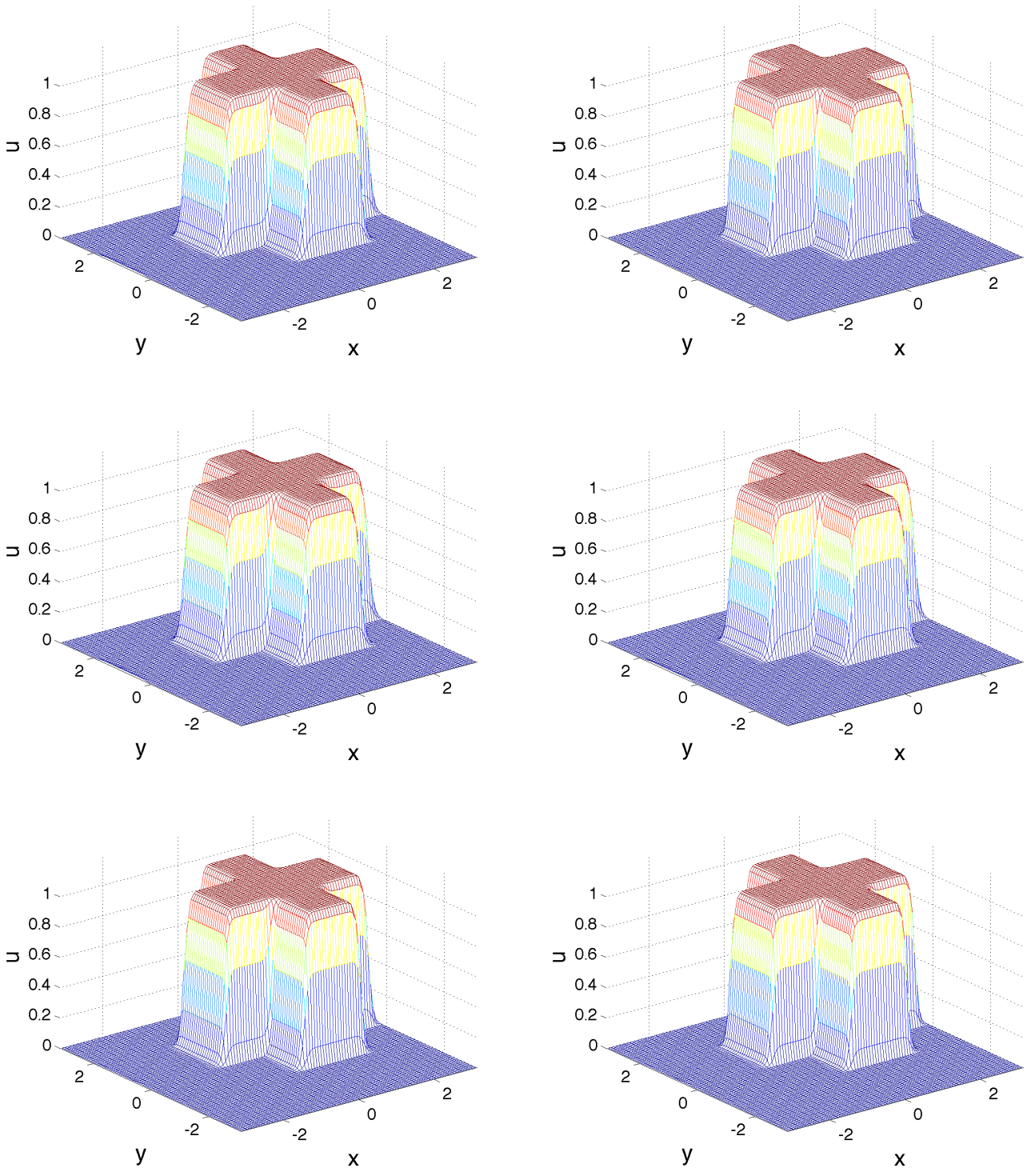

Figure 5.3: Plots of the numerical solution of equation (5.3) with $CFL = 2.2$ at $T = 1$. The initial condition is a cross shape locating in the center of the domain. The numerical mesh is 90×90. From left to right, from top to bottom are the solution from schemes with WENO3, WENO5, ENO2, WENO2, ENO3, WENO3(2) reconstructions.

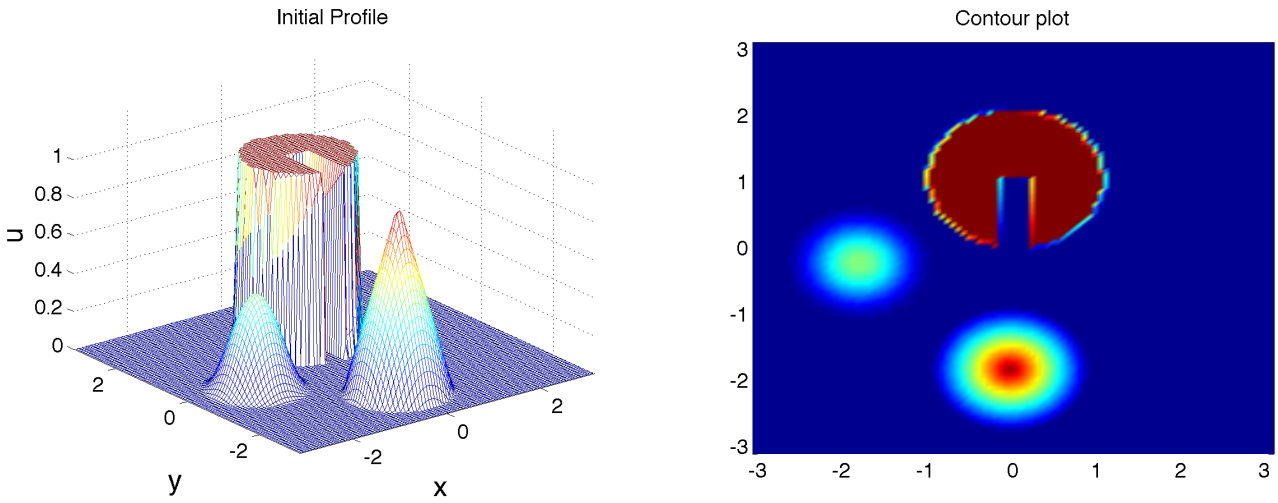

Figure 5.4: Plots of the initial profile. The numerical mesh is 100×100.

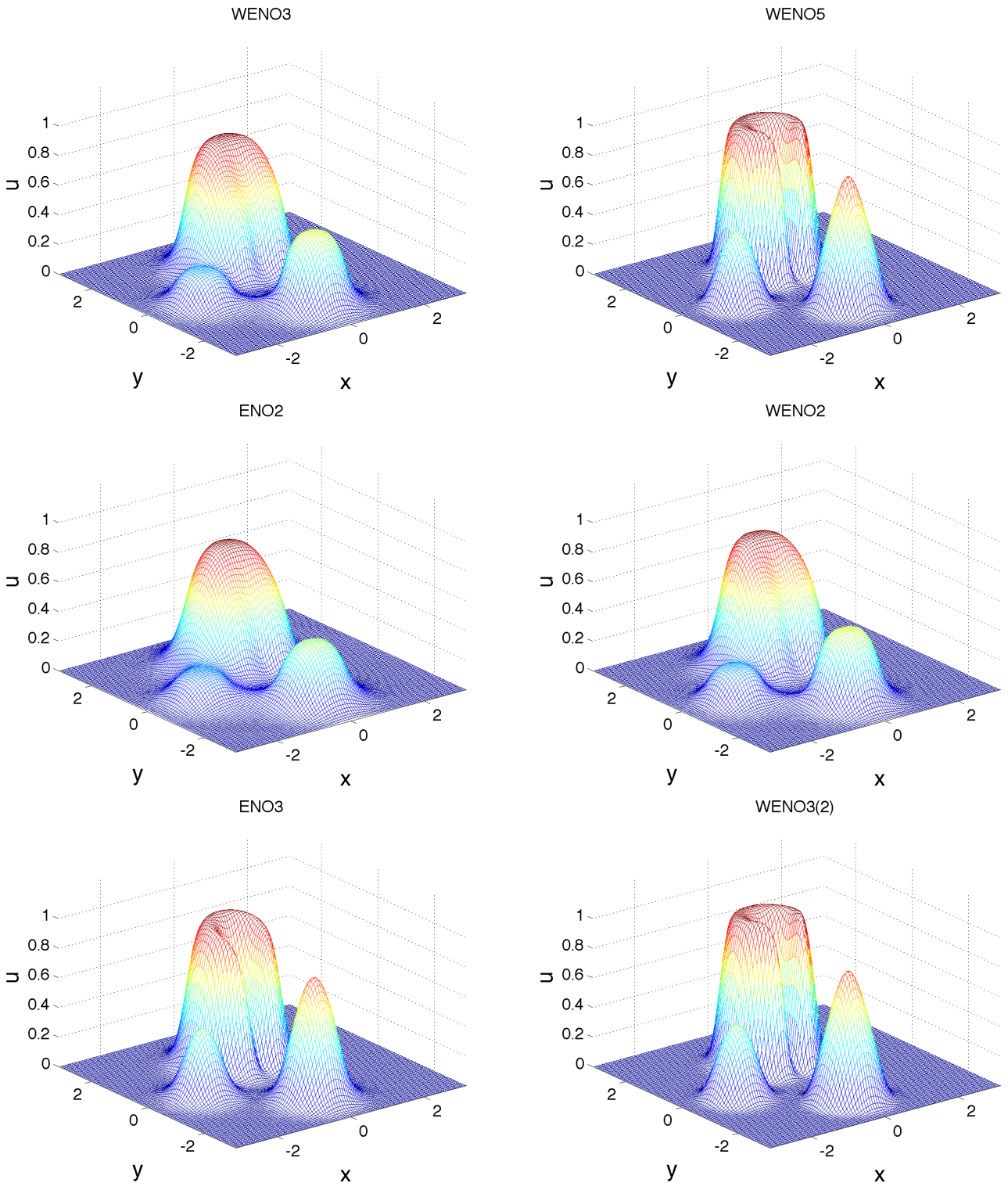

Figure 5.5: Plots of the numerical solution of for equation (5.4) with $CFL = 2.2$ at $T = 12\pi$. The numerical mesh is 100×100. From left to right, from top to bottom are the solution from WENO3, WENO5, ENO2, WENO2, ENO3, WENO3(2) reconstructions.

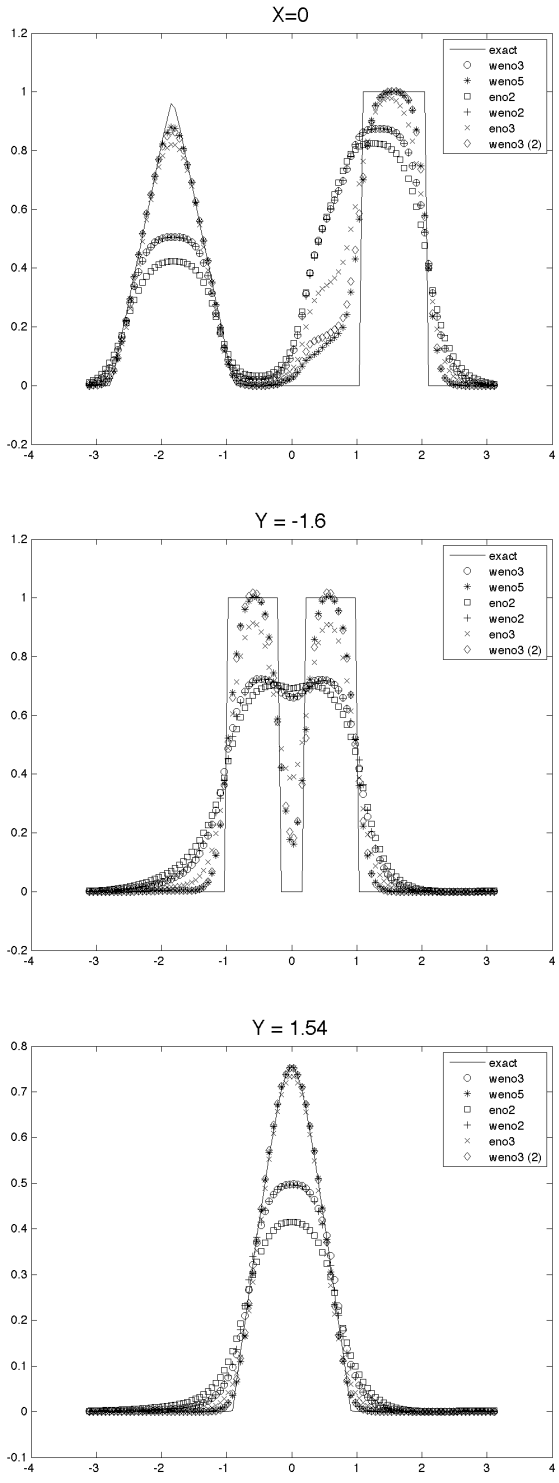

Figure 5.6: Plots of slides of numerical solution for equation (5.4) at $X = 0$ (top), $Y = -1.6$ (middle) and $Y = 1.54$ (bottom) with $CFL = 2.2$ at $T = 12\pi$. The numerical mesh is 100×100.

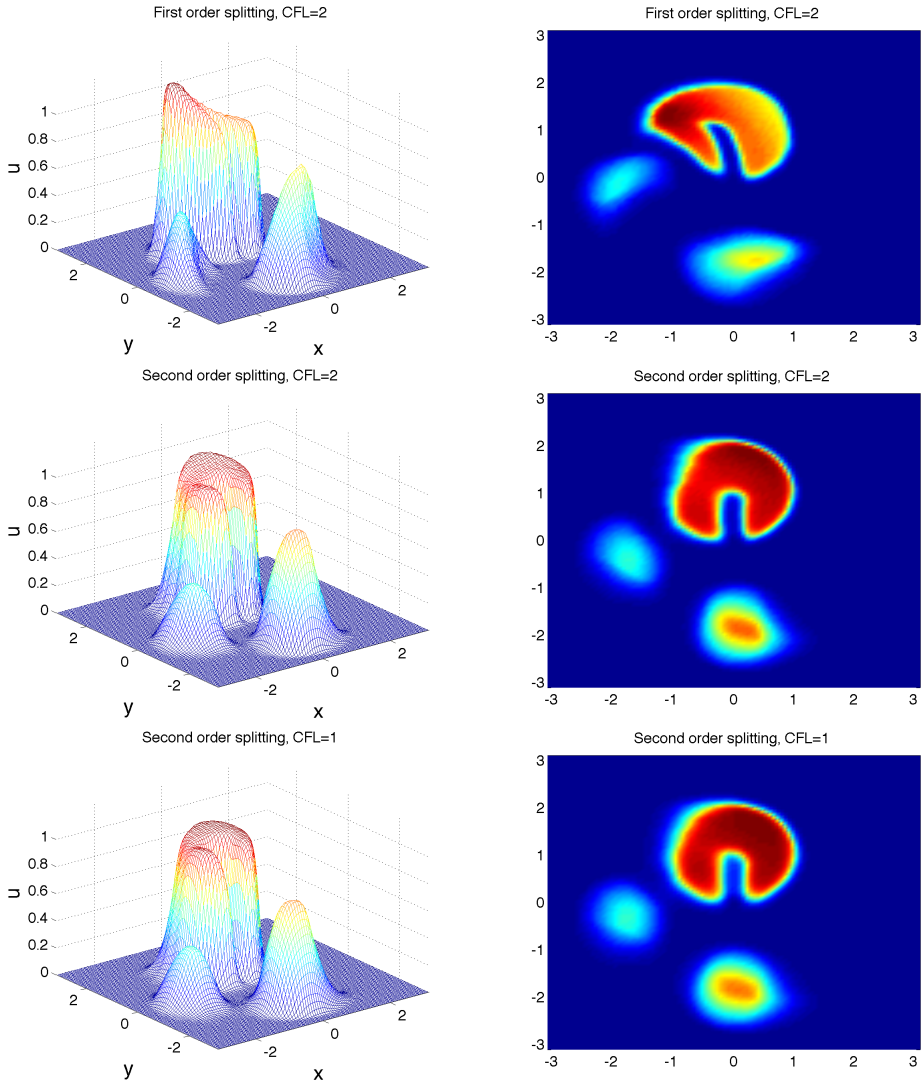

Figure 5.7: Plots of the numerical solution of for equation (5.5) with first order splitting and $CFL = 2$ (top) and $CFL = 1$ (middle); and with second order splitting and CFL $= 1$ (bottom). $T = 1.5$ and final integration time 1.5. The numerical mesh is 100×100.

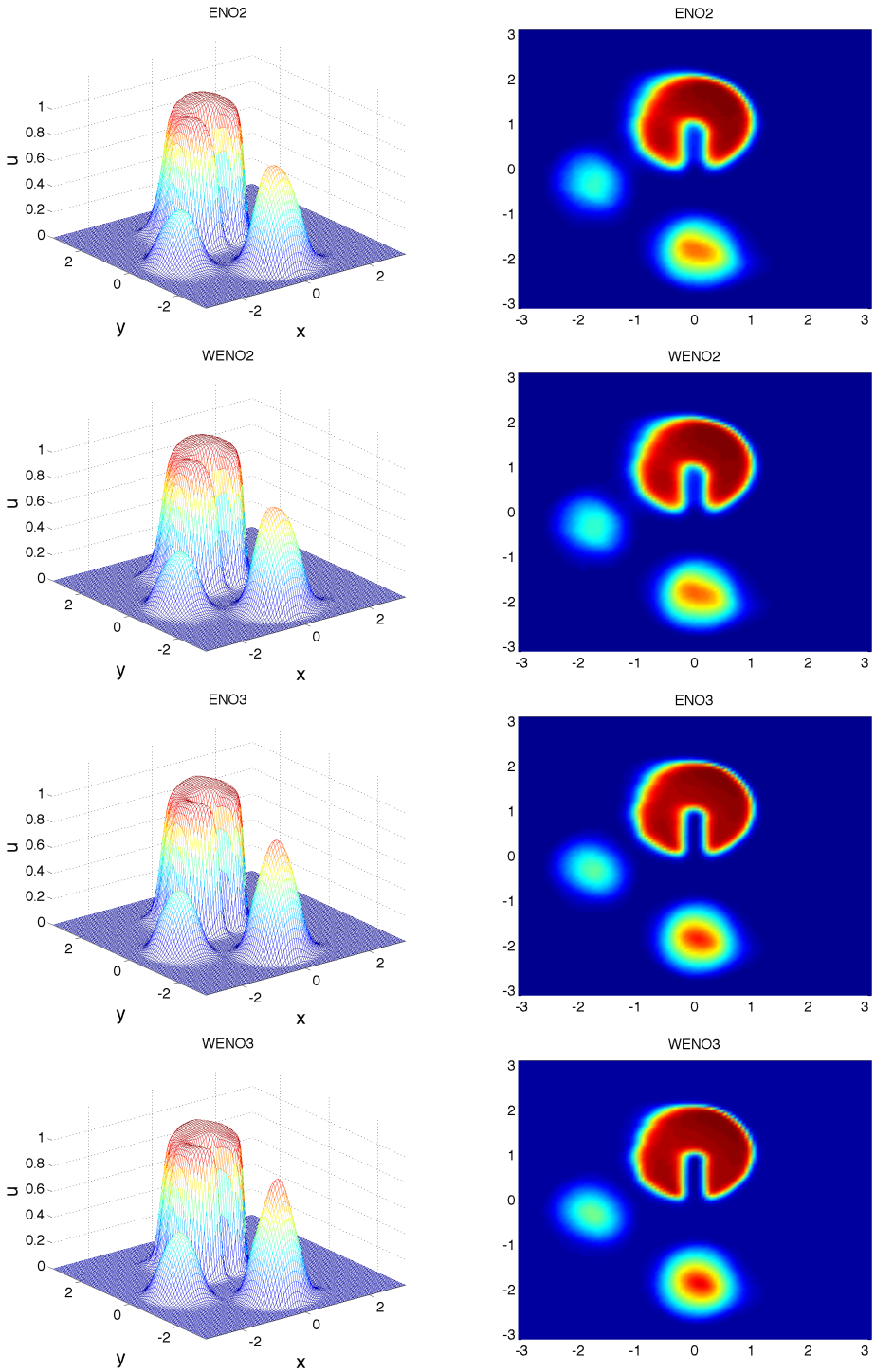

Figure 5.8: Plots of the numerical solution of schemes with second order splitting, $CFL = 1$ and with different reconstruction operators as indicated at the top of each plot for equation (5.5). $T = 1.5$ and the final integration time 1.5. The numerical mesh is 100×100.

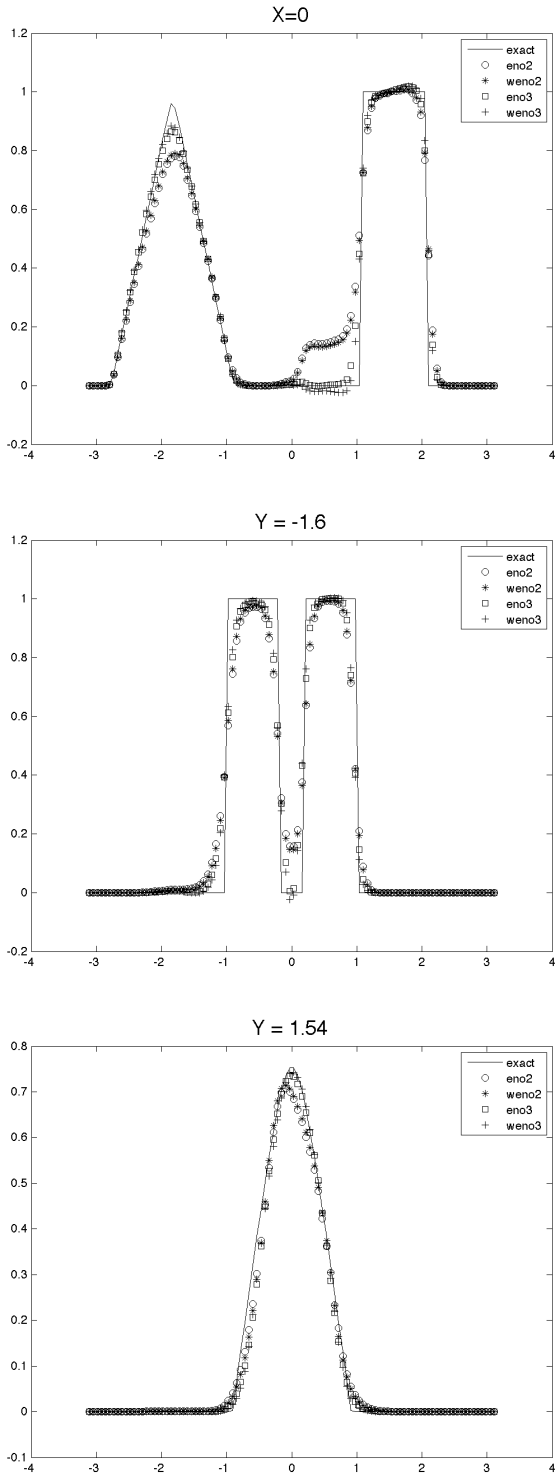

Figure 5.9: Plots of slides of numerical solution for equation (5.5) benchmarked with exact solution, at $X = 0$ (top), $Y = -1.6$ (middle) and $Y = 1.54$ (bottom) with second order Strang splitting and $CFL = 1$. The numerical mesh is 100×100.

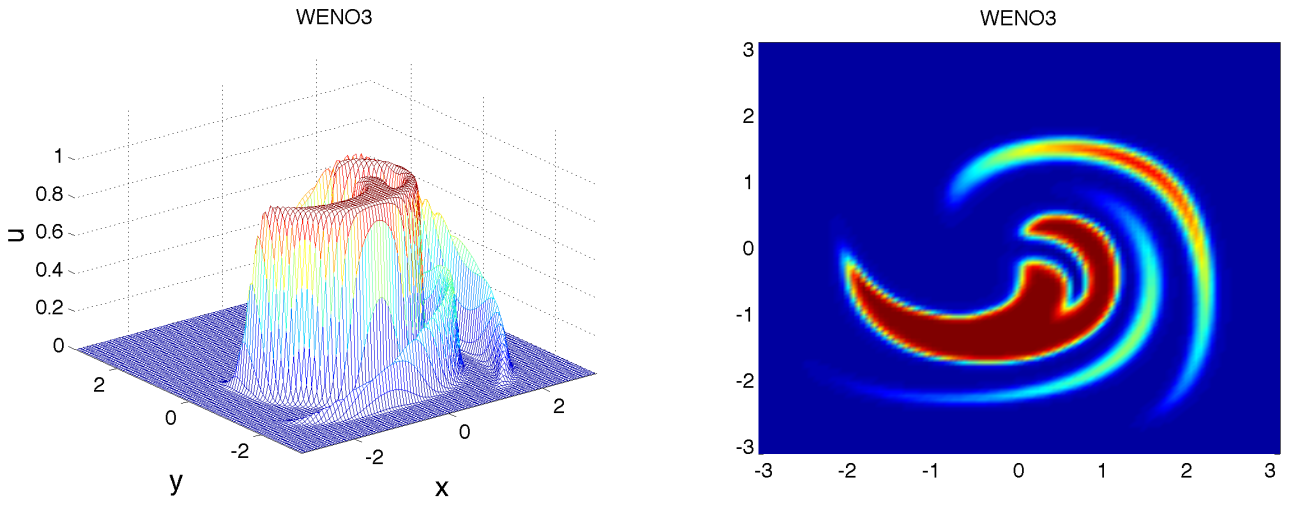

Figure 5.10: Plots of the numerical solution of schemes with WENO3 (2) reconstruction for equation (5.5) with $CFL = 1$, $T = 1.5$ and final integration time 0.75, when the initial profile is quite deformed. The numerical mesh is 100×100.

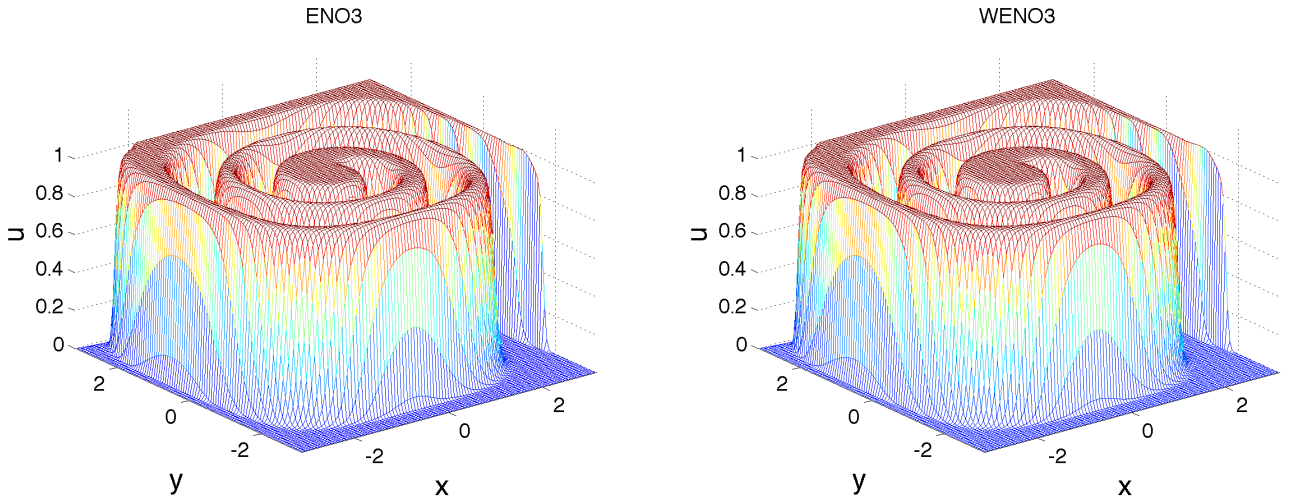

Figure 5.11: Plots of the numerical solution with ENO3 (left) and WENO3 (3) (right) reconstruction for equation (5.5) with mesh size 100×100, $CFL = 1$ and final integration time 2.5.